Climate Dynamics (2023) 60:2665–2685
https://doi.org/10.1007/s00382-022-06466-z

The mechanism linking the variability of the Antarctic sea ice extent in the Indian Ocean sector to Indian summer monsoon rainfall

Siti Syairah Atiqah Azhar[1,2] · Sheeba Nettukandy Chenoli[1,2,3] · Azizan Abu Samah[1,2,3] · Seong-Joong Kim[4] · Nuncio Murukesh[5]

Received: 5 December 2021 / Accepted: 9 August 2022 / Published online: 24 August 2022

Abstract

The study investigates the mechanism of teleconnection between the variability of sea ice extent (SIE) in the Indian Ocean sector of the Southern Ocean and the variability of Indian summer monsoon rainfall. We utilized reanalysis, satellite, in-situ observation data, and model output from the coupled model intercomparison project phase 5 (CMIP5) from 1979 to 2013. The empirical orthogonal function (EOF) and correlation analysis show that the first and third modes of principal component (PC1 and PC3) of SIE in the Indian Ocean sector during April–May–June (AMJ) are significantly correlated with the second mode of principal component (PC2) of Indian summer monsoon rainfall. The reanalysis data revealed that the changes in the SIE in the Indian Ocean sector excite meridional wave train responses along the Indian Ocean for both principal component modes. Positive (negative) SIE anomalies based on first and third EOFs (EOF1 and EOF3), contribute to the strengthening (weakening) of the Polar, Ferrel, and Hadley cells, inducing stronger (weaker) convective activity over the Indian latitudes. The stronger (weaker) convective activity over the Indian region leads to more (less) rainfall over the region during high (low) ice phase years. Furthermore, a stronger (weaker) polar jet during the high (low) ice phase is also noted. The selected CMIP5 models captured certain atmospheric teleconnection features found in the reanalysis. During AMJ, the SIE simulated by the NorESM1-M model was significantly positively correlated with Indian summer monsoon rainfall, whereas the IPSL-CM54-LR model showed a negative correlation.

Keywords Antarctic sea ice extent (SIE) in the Indian Ocean sector · High ice phase · Low ice phase · Indian summer monsoon rainfall · Convective activity

1 Introduction

Sea ice extent (SIE) is a very sensitive climate variable in polar regions, and is an essential factor in the climate system. The sea ice extent variabilities influence the global climate system, encompassing the climate of both hemispheres. Since a decade ago, researchers have studied teleconnection between Antarctic sea ice and tropical climate variability extensively. Many previous studies identified the teleconnection between the variability of the Antarctic sea ice and various atmospheric-oceanic parameters and indices, including El Niño Southern Oscillation or ENSO (Simmonds et al. 1995; Schneider et al. 2012), the Southern Annual Mode or SAM (Pezza et al. 2008, 2012; Turner et al. 2015), the Southern Indian Ocean Dipole (Nuncio et al. 2015), sea surface temperature (Rai et al. 2006, 2008; Liu et al. 2011), precipitation of the tropical Pacific (Yuan and Martinson 2000) and rainfall in China (Xue et al. 2003; Liu et al. 2018; Zhou

✉ Sheeba Nettukandy Chenoli
sheeba@um.edu.my

1 Institute of Ocean and Earth Sciences, Institute of Postgraduate Studies Building, University of Malaya, Kuala Lumpur, Malaysia

2 Research Management and Innovation Complex, National Antarctic Research Centre, University of Malaya, Kuala Lumpur, Malaysia

3 Department of Geography, Faculty of Arts and Social Sciences, University of Malaya, Kuala Lumpur, Malaysia

4 Korea Polar Research Institute, Incheon 21990, Republic of Korea

5 National Centre for Polar and Ocean Research, Ministry of Earth Sciences, Government of India, Headland Sada, Vasco Da Gama 403804, Goa, India

et al. 2021). Those studies demonstrated how the signal from the southern polar region could spread its influence across the equator (Bromwich et al. 1998; Hines et al. 2002). Based on the observed data and modeling experiments, Bromwich et al. (1998) successfully found that the removal of Antarctic sea ice causes significant changes in pressure, vertical circulation, and precipitation in the middle latitude of the Northern hemisphere (August–November). The anomaly patterns in the zonal wind, associated with temperature anomalies, cause the southern polar front jet to merge with the subtropical jet in the upper troposphere, resulting in a decrease in high-latitude low-level easterlies. The removal of Antarctic sea ice also causes large-scale precipitation to fall farther north over China in September, particularly along the coast. Furthermore, Antarctic sea ice has also been demonstrated to have a strong connection with the boreal and summer rainfall anomalies in China, in which more rainfall reaches the north of the Yellow River and lesser rainfall in the south and northeast of the Zhujiang River (Xue et al. 2003). The study also stated that as the Antarctic sea ice expands, the East Asian summer monsoon circulation will become more intense, with a decrease in sea level pressure in East Asia and an increase in sea level pressure in the North Pacific. A recent study demonstrated that autumn rainfall variability over west China is positively related to boreal summer sea ice concentrations over the southern Indian and Pacific Oceans basins. It is justified by the variation of the Lake Balkhash trough, the Asian low pressure, the position of the East Asian jet and water vapour transport (Zhou et al. 2021). However, most previous studies on the mechanism or modelling were about Arctic sea ice and the East Asian Monsoon, variability of rainfall in China and Indian summer rainfall (Wu et al. 2009a, 2009b; Guo et al. 2014; Prabhu et al. 2016, 2017; Shen et al. 2019; Zhang et al. 2021). For example, Prabhu et al. (2017) illustrated the linkage between Greenland Sea ice and India monsoon rainfall through the perturbation of atmospheric circulation by the warm sea surface temperature over the equatorial central Pacific. A recent study by Chatterjee et al. (2021) illustrated the possible relationship between summer SIE in the Kara Sea and Indian summer monsoon rainfall extreme precipitation events. The decline of SIE in the Kara Sea modulates the characteristics of the jet stream and the anomalous meridional circulation over the northwest of Europe, triggering the Rossby wave train and inducing positive upper-level as well as warm sea surface temperature anomalies in the northwestern Arabian Sea. Enhanced convection associated with warmer sea surface temperature results in anomalous upward vertical velocity over the central Indian region. While a different study (Zhang et al. 2021) shows that Barents Sea ice concentration (before winter) causes positive geopotential height anomalies over the polar region, this weakens the polar vortex and westerly winds, resulting in an indirect cyclonic anomaly over West Siberia. The circulation anomalies caused a zonal dipole pattern of preceding winter snow water equivalent anomalies in the mid-high latitudes of Eurasia (less snow water equivalent over Eastern Europe; more snow water equivalent over West Siberia), which allowed for more precipitation over Northeast China. Despite the critical role of the Antarctic SIE towards the tropical climate system, understanding the fundamental mechanism of the connection between a change in Antarctic SIE and Indian summer monsoon rainfall is still limited. The absence of teleconnection references and other factors (i.e. nature of the relationship, ocean, atmosphere), particularly the physical and dynamic mechanisms, has restricted researchers from exploring this topic using model simulation. Moreover, Mahlstein et al. (2013) noted that coupled model intercomparison project phase 5 (CMIP5) models need to improve the representation of processes in the atmosphere and ocean that affect trends in the Antarctic sea ice area to simulate the observed Antarctic sea ice trend. Thus, the models have to be treated with caution.

Indian summer monsoon rainfall is an interannual event that usually occurs from June until September. It is one of the major weather patterns that dominate the Indian climate. The monsoon rainfall is frequently accompanied by extreme floods or drought in different regions of India. The range of monsoon variability can significantly impact economic growth, society, and the environment (Gadgil et al. 2006; Clift and Plumb 2008). As mentioned by Pritpal (2018), monsoon rainfall is influenced by many factors, such as the position of the semi-permanent monsoon trough, sea surface temperature and Mascarene high, but the other contributing factors behind the variations are still unknown. In our previous study (Azhar et al. 2020), we successfully showed a teleconnection between the SIE in the Indian Ocean sector with the Indian summer monsoon rainfall through the modulation of the Mascarene high. Azhar et al. (2020) revealed that the Mascarene high strengthens (weakens) during the high (low) ice phase years and leads to more (less) Indian summer monsoon rainfall. Mascarene high is also strongly associated with regional climate anomalies in the southern hemisphere. Xulu et al. (2020) documented that Mascarene High has a vital role in weather and climate variability over Southern Africa. They noted that anomalous rainfall and temperature events over the African subcontinent is linked to the atmospheric blocking by Mascarene High. Rehman et al. (2019) showed that the strengthening of the Indian Ocean subtropical high has a significant impact on the seasonal variability of precipitation over Tasmania). In a recent study by Bajish et al. (2021) demonstrated that the sea ice over the Bellingshausen–Amundsen Sea sector has a negative connection with the Indian summer monsoon rainfall during the austral summer. This is due to the existence of a cyclonic (anticyclonic) wind pattern over the Ross Sea

and Bellingshausen–Amundsen Sea sector during excess (deficit) periods, which leads to the anomalous positive (negative) sea air temperature and sea surface temperature that ease anomalous negative (positive) sea ice condition in the Bellingshausen–Amundsen Sea sector. In this study, we attempt to find the possible mechanisms for the teleconnection between the SIE in the Indian Ocean sector and the Indian summer monsoon rainfall in terms of atmospheric circulation, especially at the upper troposphere. It is crucial to understand how anthropogenic forgings impact and modify the teleconnection signals in the future. The climate models are an essential tool for understanding the mechanisms of tropical polar teleconnections and their projected changes (Li et al. 2021). Despite this, the models suffer from biases and uncertainties, preventing an accurate assessment of the future projections. Therefore, this study also assessed selected CMIP5 models in simulating the observed teleconnection pattern of the Antarctic SIE and Indian summer monsoon.

This paper is divided into the following sections. Section 2 describes the various forms of data and the methodology used in the study. Section 3 and Sect. 4 provide results and discussion on the possible mechanism of the teleconnection using reanalysis and model simulation data. The last section presents the conclusions of this study and also future work.

2 Data and methodology

2.1 Observations and reanalysis data

1. The monthly sea ice concentration was retrieved from Met Office Hadley Centre Global Sea Ice and Sea Surface Temperature (HadISST, Rayner et al. 2003) data. It contains monthly mean fields on the globe with a spatial resolution of 1.0º × 1.0º latitude–longitude grids from January 1870 to December 2020. The SIE in the Indian Ocean sector (from 20° E to 90° E) was computed when the sea ice concentration exceeded 15%. It is worth noting here that the SIE in the Antarctic in this sector had shown significant positive trends in most of the months during the period 1979–2013 (Simmonds 2015).
2. The monthly reanalysis datasets of mean geopotential height, vertical velocity, and zonal and meridional winds at nine pressure levels (1000 hPa, 925 hPa, 800 hPa, 700 hPa, 600 hPa, 500 hPa, 400 hPa, 300 hPa,200 hPa and 100 hPa) were compiled from the European Centre for Medium-range Weather Forecasting, ERA-Interim reanalysis data. The period of the data was from January 1979 to December 2013, with a spatial resolution of 0.75° × 0.75° latitude–longitude grids. ERA-Interim has been utilized for the analysis as this research study was started before the availability of ERA5.
3. The monthly Global Precipitation Climatology Project data with a spatial resolution of 2.5° × 2.5° latitude–longitude grids was used. This data is available from January 1971 to December 2013.
4. The monthly mean interpolated dataset of Outgoing Longwave Radiation (OLR) from the National Center for Atmospheric Research online archive was also used. The data is available from June 1974 until January 2017 with a spatial resolution of 2.5° × 2.5° latitude–longitude grids.
5. The authors noted that the ERA5 data assimilation system has significant modifications, including higher spatial and temporal resolutions compared to ERA-Interim. However, this research project started much earlier than the availability of ERA5. The lock-down situation due to COVID-19 further delayed the project.

2.2 Description of CMIP5 models

CMIP5 models were used in this study to assess the capability of the model in representing the teleconnection pattern found in the reanalysis data. The models were selected based on their ability to simulate sea ice extent (NorESM1-M, MPI-ESM-MR, GFDL-CM2.1, IPSL-CM54-LR, ACCESS 1.0 and ACCESS 1.3), and these models were proven to simulate the SIE comparable to the observations (Collins et al. 2008; Turner et al. 2013; Bi et al. 2013; Rashid et al. 2013; Uotila et al. 2014; Yang et al. 2016), and reanalysis results. Holmes et al. (2019) successfully identified the group of models close to the observed ice area. There are ACCESS and CMCC models, MRI-CGCM3, and NorESM1-M, that simulate ice areas reasonably well year-round. However, most of the earlier studies used the period 1979–2005; differing trends in models and observations (Zunz et al. 2013) mean that the later 2003–2010 period generally results in decreased modeled ice coverage and increased observed ice coverage. The details of the CMIP5 models used in this study are listed in Table 1. Similarly, the SIE in the Indian Ocean sector was computed when the sea ice concentration exceeded 15%.

The simulation of atmospheric historical output has different vertical hybrid levels and horizontal resolutions from approximately 2.5° × 1.9°, while the sea ice output has a horizontal resolution of 0.5°. The simulation of historical monthly output is available from January 1850 to December 2005. Therefore, for comparison purposes and to have consistent periods with the reanalysis data, the six years (2006–2012) of simulation data from the RCP 4.5 experiment were used. The RCP 4.5 experiment is known as a long term and intermediate stabilization scenario where total radiative forcing is stabilized around 2050 by employing a

Table 1 Namelist, resolutions, parameters and ensemble numbers of CMIP5 models were used in this study

Nu	Models	Institution/Organization	Country	Parameters	Resolution (sea ice/atmosphere)	Ensemble members
1	NorESM1-M	Norwegian Climate Centre (NCR)	Norway	Sea ice concentration; Geopotential height, Zonal wind, Meridional wind, Vertical velocity, Ongoing longwave	0.5 × 0.5/2.5 × 1.9	3
2	MPI-ESM-MR	Max-Planck Institute (MPI)	Germany		0.5 × 0.5/2.5 × 1.9	3
3	GFDL-CM2p1	Geophysical Fluid Dynamics Laboratory (GFDL)	USA		0.5 × 0.5/2.5 × 1.9	10
4	IPSL-CM54-LR	Institute Pierre-Simon Laplace (IPSL)	France		0.5 × 0.5/3.75 × 1.9	6
5	ACCESS 1.0 & ACCESS 1.3	Commonwealth Scientific and Industrial Research Organization (CSIRO), Bureau of Meteorology (BOM)	Australia		0.5 × 0.5/1.25 × 1.875	3

range of technologies and strategies for reducing greenhouse gas emissions. It represents an intermediate scenario where the temperature increase is still within 2 °C, which is recognized as the threshold at which climate change becomes dangerous. Furthermore, RCP4.5 is derived from its own reference or no climate policy scenario. This reference scenario is unique to RCP4.5 and differs from RCP8.5 as well as from RCP6 and RCP2.6 (Moss et al. 2010; Thomson et al. 2011). It also employs updated historical data series by calibrating up to the year 2000 (Lamarque et al. 2010).

In addition, to assess the performance of the CMIP5 models in reproducing sea ice and monsoon linkages, we compared the CMIP5 models output with the ERA-Interim reanalysis datasets, which are considered the most reliable reanalysis datasets (Simmons et al. 2014) before the availability of ERA5 dataset as mention above.

2.3 Method

The techniques of correlation, spatial regression, composite analysis, and empirical orthogonal function (EOF) analysis were performed in this study. An EOF analysis was carried out to analyze the most important patterns of the SIE and Indian summer monsoon rainfall variations. The spatial and temporal functions are used to examine the sea ice variability in the Indian Ocean sector and precipitation over the Indian region. A correlation analysis was performed in order to identify which sea ice modes are significantly correlated with Indian summer monsoon rainfall modes. The composites are constructed based on the significant values of the correlation coefficient between the modes of the principal component. Additionally, the wave activity flux formulated by Takaya and Nakamura (2001) was utilized to identify the possible routes of wave propagation. The modified script based on the GrADS script was used to calculate wave activity flux (http://www.atmos.rcast.utokyo.ac.jp/nishii/programs/index.html). The vertical profiles of atmospheric wind velocity were also used to investigate the atmospheric circulation patterns from the surface to the upper troposphere.

The Indian summer monsoon rainfall is defined by the composite month of June–July–August–September (JJAS). The high (low) ice phase years were defined based on the absolute and normalized value of principal component of AMJ SIE in the Indian Ocean sector is greater than 1 (lower than − 1). The study area of this research is similar to our previous study (shown in Fig. 1 of Azhar et al. 2020).

3 Results and discussion

3.1 Possible linkage mechanisms: how does SIE in the Indian Ocean sector affect Indian summer monsoon rainfall?

The relationship between Antarctic sea ice and Indian summer monsoon rainfall has been reported in several studies (Dugam et al. 2004; Prabhu et al. 2009; Azhar et al. 2020). In our previous study (Azhar et al. 2020), we showed that SIE in the Indian Ocean during April–May–June (AMJ) is the most significantly positively correlated with the Indian summer monsoon rainfall. In order to get a better understanding of this relationship, the EOF analysis was performed for the SIE during AMJ and precipitation during JJAS datasets from 1979 to 2013 (Fig. 1). The first three leading EOF modes of SIE during AMJ for 35 years are present in Fig. 1a–c. The first EOF (EOF1) mode explains 40.47% of the total variance. The spatial pattern of EOF1 shows negative anomalies of SIE over the entire Indian Ocean sector. The second EOF (EOF2) mode explains 17.03% of the variance and has positive and negative anomalies of SIE over the west and east of the Indian Ocean sector. The third EOF (EOF3) mode explains 8.40% of the total variance, and it is characterized by the spatial pattern of a positive anomaly at the centre and a negative anomaly over the east and west of the sector. More

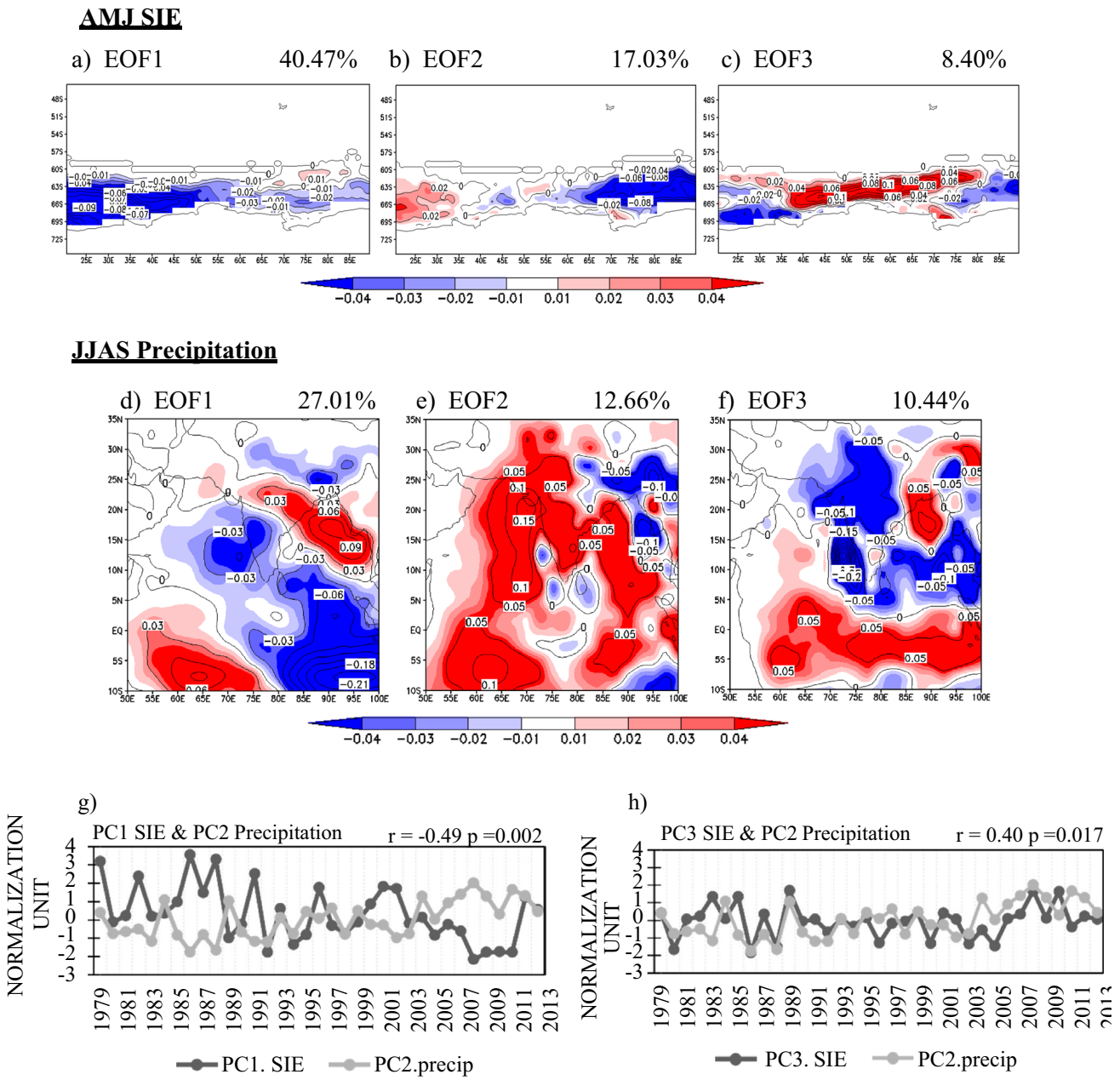

Fig. 1 The spatial pattern of three leading EOF modes of SIE (**a**–**c**) (unit: %) in AMJ and precipitation (**d**–**f**) (unit: mm/year) in JJAS. The correlation between the **g** PC1, **h** PC3 time series of AMJ SIE in the Indian Ocean sector (black) with the PC2 time series of precipitation over the Indian region (grey) from 1979 to 2013, statistically significant at $p < 0.05$

SIE appears in the centre and north-western of the region, whereas less loading is shown in the west and east near the coast of the sector. Similarly, the first three leading EOF modes of precipitation during JJAS accounted for 27.01%, 12.66% and 10.44%, respectively, as in Fig. 1d–f. The spatial pattern in EOF1 illustrated positive precipitation anomalies over north Peninsular India, extending over the Bengal Bay and the western Indian Ocean. In contrast, negative rainfall anomalies were seen over the southwest of Peninsular India, the eastern Indian Ocean, and northern India. Meanwhile, the spatial pattern of EOF2 shows the dominant features of positive rainfall anomalies over the Indian region, the Arabian Sea, and Bengal Bay. In contrast to the EOF2 mode, the spatial pattern in EOF3 shows negative anomalies over the Indian region and Bengal Bay, whereas positive anomalies are seen over the Indian Ocean. The analysis was continued by correlating the PCs of the EOF modes of AMJ SIE and JJAS precipitation. A summary of the results is tabulated in Table 2. The results show that the first mode principal component (PC1) and third mode principal component (PC3) of

Table 2 Summary of the correlation coefficient between the PC's time series of AMJ SIE in the Indian Ocean sector and PC's time series of JJAS precipitation from 1979 to 2013

		Precipitation		
		P1.precip	P2.precip	P3.precip
SIE in the Indian Ocean sector	P1.sie	− 0.17	**− 0.49***	− 0.12
	P2.sie	− 0.18	− 0.28	− 0.09
	P3.sie	0.22	**0.40***	− 0.01

The bold values indicates the p value statistically significant at *p < 0.05

AMJ SIE are significantly correlated with the second mode principal component (PC2) of precipitation. The table shows that PC1 of AMJ SIE has a statistically significant negative correlation with PC2 precipitation, with a correlation coefficient of $r = -0.49$ ($p < 0.05$) (see Fig. 1g). The PC3 of AMJ SIE has a positive correlation with the PC2 precipitation with a statistically significant correlation coefficient of $r = 0.4$ ($p < 0.05$) (see Fig. 1h). Both values indicate that SIE in the Indian Ocean sector during AMJ significantly impacts the Indian summer monsoon rainfall. In fact, both the patterns have some similarities; EOF1 depicts negative sea ice anomalies in the Indian Ocean sector, while positive anomalies characterize EOF3. However, in the EOF3, negative and positive sea ice anomalies can be noticed near the western and eastern boundaries. This suggests that when the EOF time series is positive for EOF1/EOF3, the Indian Ocean sector will mainly be characterised by negative/positive sea ice anomalies. The temporal patterns of these two EOFs are also different (Fig. 1g, h). EOF1 time series depict a negative trend (Fig. 1g), while EOF3 time series do not show any trend (Fig. 1h). This suggests that these two patterns could result from different processes but have a nearly similar manifestation on sea ice. The negative trend seen in EOF1 time series indicates an increase in sea ice anomalies in the Indian Ocean sector. Therefore, for an in-depth analysis of this relationship, we selected PC1 and PC3 of AMJ SIE to identify the high and low ice phases. The high and low phase years are categorized based on the absolute and normalized values of PC1 and PC3 of AMJ SIE in the Indian Ocean sector ≥ 1 or ≤ -1. The list of high and low ice phase years for each principal component of AMJ SIE is tabulated in Table 3. By high/low ice phase years, we mean the presence of positive/negative sea ice anomalies in the spatial patterns for EOF1 and EOF3.

As mentioned earlier, the statistical relationship was well established in previous studies, including Azhar et al. (2020). Still, the mechanisms behind the connection have not been thoroughly investigated, especially through the circulation at the upper troposphere level. As an extension of the previous study, the contour of geopotential height and wave activity flux at 250 hPa during May–Jun–July (MJJ) were analyzed to diagnose any potential wave energy propagation. Figure 2 displays the spatial regression of geopotential height at 250 hPa level for 35 years superimposed with the composite differences composite difference of wave activity flux corresponding to the PC1 (Fig. 2a) and PC3 (Fig. 2b) time series of AMJ SIE in the Indian Ocean sector. At 250 hPa level, the contour of the geopotential height anomaly exhibits a tripole structure over the Indian Ocean for both principal component modes. Figure 2a illustrates that positive anomalies over the polar region, negative anomalies over the middle latitudes, and positive over the tropics from about 20° S to 10° S. The composite difference of wave activity flux is seen propagating southward from the tropics towards the polar region in two paths. One is from South Australia, and the other is from the western Indian Ocean near 30° S. Both propagated towards the middle latitudes at about 50º S and continued propagating towards the polar region. Furthermore, the wave train appears to diverge into the area near the Mascarene high and modify the low-level circulation over that region, enhancing the low-level convergence (Ogwang et al. 2015; Jin et al. 2017) during the low ice phase years of the PC1 time series of EOF1. In contrast, opposite features of the geopotential height anomaly are shown in Fig. 2b, where a negative anomaly appears in the Indian Ocean sector of the Southern Ocean, a positive anomaly from the middle towards the tropics, from about 50° S to 30° S and a negative anomaly from about 30° S to 10° S over the tropics. The composite difference of wave activity flux featured a northward propagating wave train from the polar region towards the middle latitudes as well as the tropics in two pathways. Originated from the Indian Ocean sector, one propagated towards the middle latitude along the centre of the Indian Ocean at about 35° S, particularly over the Mascarene high region, and continued propagating toward the tropics at about 15° S. Another one travelled eastwards to the Australian region. While the

Table 3 Summary of high and low ice phase years corresponding to PC1 and PC3 time series of AMJ SIE in the Indian Ocean Sector

PC's time series of AMJ SIE in the Indian Ocean sector	High ice phase years	Low ice phase years
PC1	1989, 1992, 1994, 2008, 2009, 2010,2011 **(7)**	1979, 1982, 1986, 1987, 1988,1991, 1996, 2001, 2002,2012 **(10)**
PC3	1983, 1985, 1989, 2008, 2009, 2010 **(6)**	1980, 1986, 1988, 1996,2000,2003, 2005 **(7)**

The bold values inside the ( ) indicate the number of years

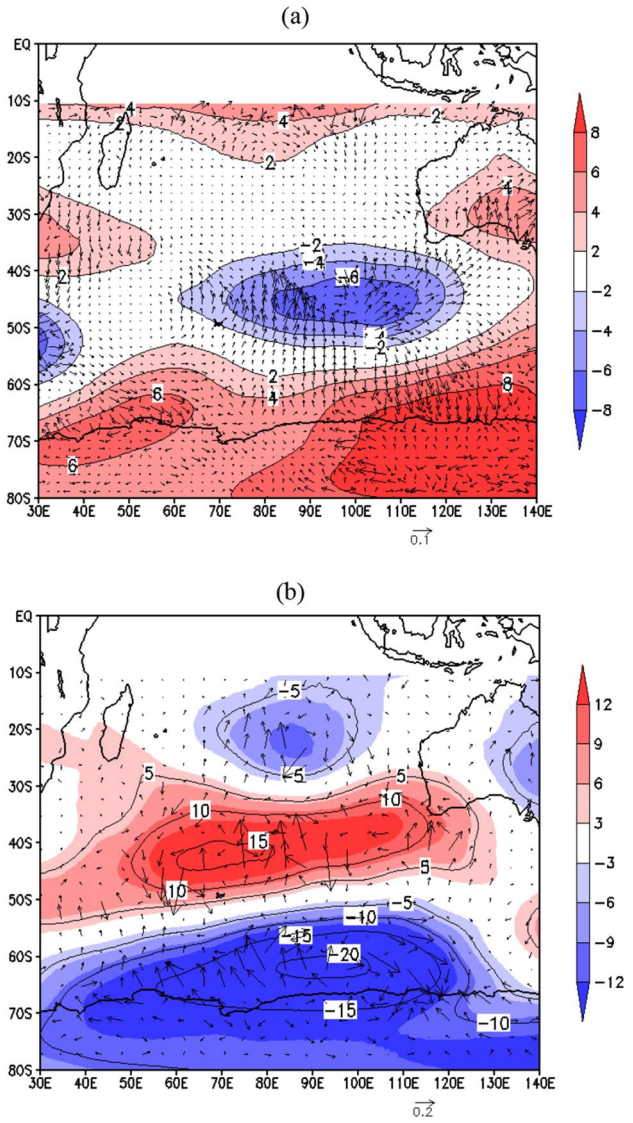

Fig. 2 The regressed anomalous contour of geopotential height (shaded and contour, unit: m) for 35 years superimposed with the composite difference of wave–activity flux (unit: m^2s^{-2}) for high and low phases of EOF1/EOF3 corresponding to **a** PC1, **b** PC3 time series of AMJ SIE in the Indian Ocean sector during MJJ at 250 hPa

wave train in Fig. 2b seems to converge into the Mascarene high area, and increases the low-level divergence during the high ice phase years of the PC3 time series of EOF3. It may be noted that the geopotential height anomaly patterns is somewhat similar but in opposite phases for both the EOFs discussed. This is due to the fact in positive phases of EOF1/EOF3 is characterized by negative/positive sea ice anomalies. This in turn, means that positive sea ice anomalies (high ice phase) in both the EOFs, will result in similar wave propagation. Hence, stronger easterlies emerging from the Mascarene high can be expected over the south Indian Ocean, contributing to the intense cross-equatorial flow and strong south westerlies over the India region. Consequently, there was increased rainfall in the Indian region when sea ice anomalies are positive in the Indian Ocean sector. Our previous study also discussed this feature (Azhar et al. 2020) and agreed with Sun et al. (2009). Both studies revealed that the development of the meridional teleconnection wave train is strongly related to Mascarene high variability and wind circulation at the lower level. This circulation pattern between lower and upper levels clearly indicates the effect of SIE variability towards the Mascarene high, influencing the rainfall over the Indian region. Additionally, the anomalous 250 hPa geopotential height is also accompanied by a change in the polar front and subtropical jet.

Figure 3 represents the vertical profile of the composite difference of the zonal wind average corresponding to the PC1 (Fig. 3a) and PC3 (Fig. 3b) time series of AMJ SIE in the Indian Ocean sector. Here too, both the composites represent the opposite phases since both EOF1 and EOF3 more or less represent opposite phases of sea ice anomalies in the Indian Ocean sector. The arguments presented are similar to those in Fig. 2. Simmonds and Budd (1991) explored the sensitivity of the Southern Hemispherical circulation to changes in response to the fraction of open water in the polar ice packs based on the General Circulation Model (GCM) experiments. Experiments with 50 and 100% fraction of open water in the pack ice show anomalous easterlies between 40° S and 60° S with westerly anomalies further to the south. However, the structure for the 80% fraction was similar, except that the band of easterly tropospheric anomalies does not extend to the surface. The composite difference of zonal wind average (Fig. 3) exhibits barotropic nature, and the features and structure appear similar to the structure in Simmonds and Budd (1991). Figure 3a shows that the maximum negative and positive anomalies of the zonal wind average are located at the latitudes of 58° S and 38° S at an altitude of around 400 hPa and 250 hPa, respectively. The difference in the maximum anomalies of the high and low phase years is − 2 ms^{-1}, indicating the polar front jet is weaker during the low ice phase years of the PC1 time series of EOF1. While for the subtropical jet, there is only a slight difference in the value of maximum anomalies in both phases, indicating minimal impacts on the subtropical jet compared with the polar front jet. Figure 3b shows the opposite features where the maximum positive and negative anomalies of zonal wind averages are located at the latitudes of 56° S and 36° S at an altitude of around 450 hPa and 150 hPa, respectively. The difference in the maximum anomalies is 4 ms^{-1}, indicating the polar front jet is stronger during the high ice phase years of the PC3 time series of EOF3. Similarly, the subtropical jet also has minimal impact in the both phases. According to Carvalho et al. (2005), the variability of the zonal wind anomalies in the upper troposphere is closely related to the jet stream variability that

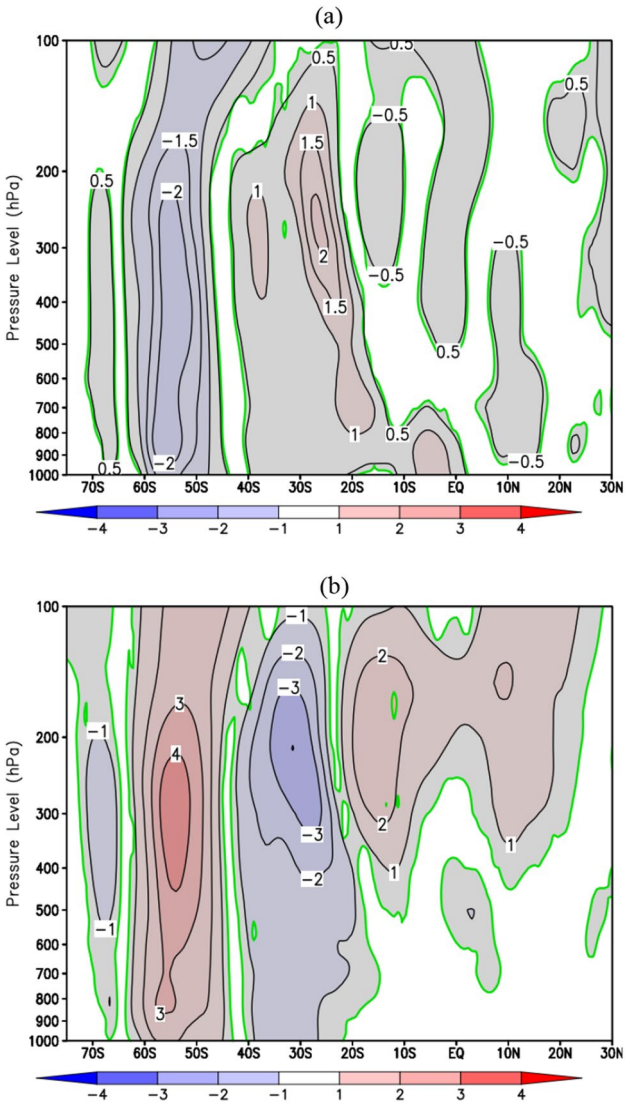

Fig. 3 The vertical profile of composite difference of zonal wind average for high and low phases of EOF1/EOF3 (unit: ms^{-1}, averaged over 55° E–85° E) corresponding to **a** PC1, **b** PC3 time series of AMJ SIE in the Indian Ocean sector. The shaded area in grey and solid lines in green are statistically significant at $p < 0.05$

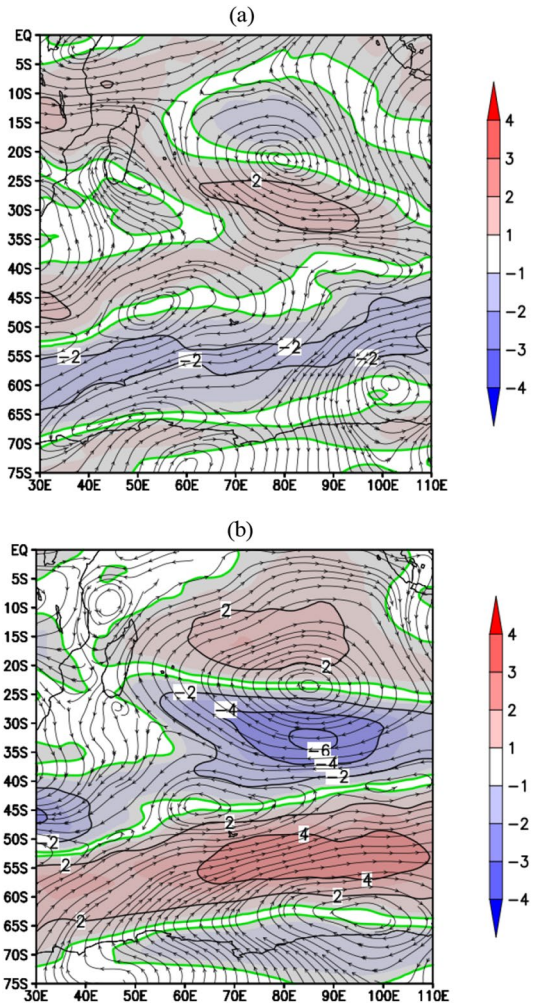

Fig. 4 The composite difference of zonal(shaded) wind (streamlines) anomalies at 250 hPa (unit: ms^{-1}) for high and low phases of EOF1/EOF3 and corresponding to **a** PC1, **b** PC3 time series of AMJ SIE in the Indian Ocean sector. The shaded area in grey and solid lines in green are statistically significant at $p < 0.05$

influences the atmospheric circulation features. Also, the concurrent variation of the polar front jet and subtropical jet serves as a critical indication of interaction between low and high latitude circulation systems (Luo et al. 2015).

This can be clearly seen in Fig. 4, which shows the composite difference of the zonal wind anomalies superimposed with the wind anomalies corresponding to the PC1 (Fig. 4a) and PC3 (Fig. 4b) time series of AMJ SIE in the Indian Ocean sector at 250 hPa during MJJ. Figure 4a, b of the zonal wind anomalies for both principal component modes show a quadrupole pattern distribution from the high to low latitudes at 250 hPa. The zonal wind anomalies in Fig. 4a show a positive anomaly over the small parts of the west and east polar regions, a negative anomaly over the high latitudes from about 65° S to 55° S, a positive anomaly from about 45° S to 25° S, and a negative anomaly from about 20° S to 10° S. These features are associated with an intense cyclonic wind anomaly at about 50° S and an intense anticyclonic wind anomaly at about 60° S and 20° S. These cyclonic and anticyclonic wind anomalies imply a strong divergence and convergence anomaly at a lower level (Chen et al. 2019; Zhao et al. 2021) during the low ice phase years of the PC1 time series of EOF1. Figure 4b shows the opposite features of zonal wind anomalies (positive–negative–positive–negative) as well as the wind anomalies. The zonal wind anomalies show a negative anomaly in the polar region, a positive anomaly in high latitudes from about 70° S to 55° S, a negative anomaly in middle latitudes from about 50° S to 25° S, and a positive anomaly in lower latitudes

from about 20° S to equatorial. These features are associated with an intense anticyclonic wind anomaly over the southwest of the Indian Ocean at about 50° S, implying a more robust divergence anomaly at 250 hPa, leading to more subsidence and more substantial surface convergence. Also, another intense cyclonic wind anomaly can be seen over the polar region at about 70° S and the centre of the Indian Ocean at about 20° S. This cyclonic wind anomaly implies a strong convergence anomaly associated with a strong divergence anomaly at the lower level (Chen et al. 2019; Zhao et al. 2021) during the high ice phase years of the PC3 time series of EOF3. It is evident that the high and low ice phase years as inferred from EOF1 and EOF3 influences the middle latitude weather patterns by altering the jet stream characteristics due to increased polar-middle latitude temperature gradient as well as other factors such as the strengthening of the westerly winds. The poleward migration of the westerly jet in austral summer is also associated with greenhouse gas emissions and ozone-depleting substances (Cohen et al. 2014; Screen et al. 2018; Blackport and Screen, 2020). Therefore, the alteration of the zonal wind anomalies during both phases suggests an upper and lower level meridional teleconnection between the SIE in the Indian Ocean sector and Indian summer monsoon rainfall. Consistent with Hoskins and Ambrizzi (1993) findings, it can be concluded that upper-level zonal wind could operate as a teleconnection feature, allowing for a more detailed interpretation of propagation patterns from middle latitudes to the tropics.

Besides, the variabilities of jets are strongly related to the variability of the Ferrel cell (Sun et al. 2009; He et al. 2011) and the position of the Hadley cell (Shi et al. 2016; Manzel et al. 2019). The Ferrel cell and Hadley cell play vital roles in contributing to the general circulation between the middle and higher latitudes and the climate of the tropics and subtropics (Li and Wang, 2003; Nguyen et al. 2013; Hu et al. 2018; Rudeva et al. 2019). Hudson et al. (2001) suggested that changes in sea level pressure are verified by vertical velocity changes. Positive sea level pressure anomalies result from the strengthening and southward expansion of the subtropical high-pressure belt. The increased uplift in the ascending limb of the Ferrel cell is related to decreases in pressure. Details of the atmospheric circulation related to the variability of the local Ferrel cell and Hadley cell are discussed in the next section.

3.2 Vertical profile of meridional circulation: polar cell, ferrel cell and hadley cell

The variation in meridional circulation plays a significant role in climate change (Hu and Fu, 2007), and it is also the main factor contributing to the polar and tropics connection (Liu et al. 2002). However, the process is not well understood, especially in terms of how the variability of SIE is

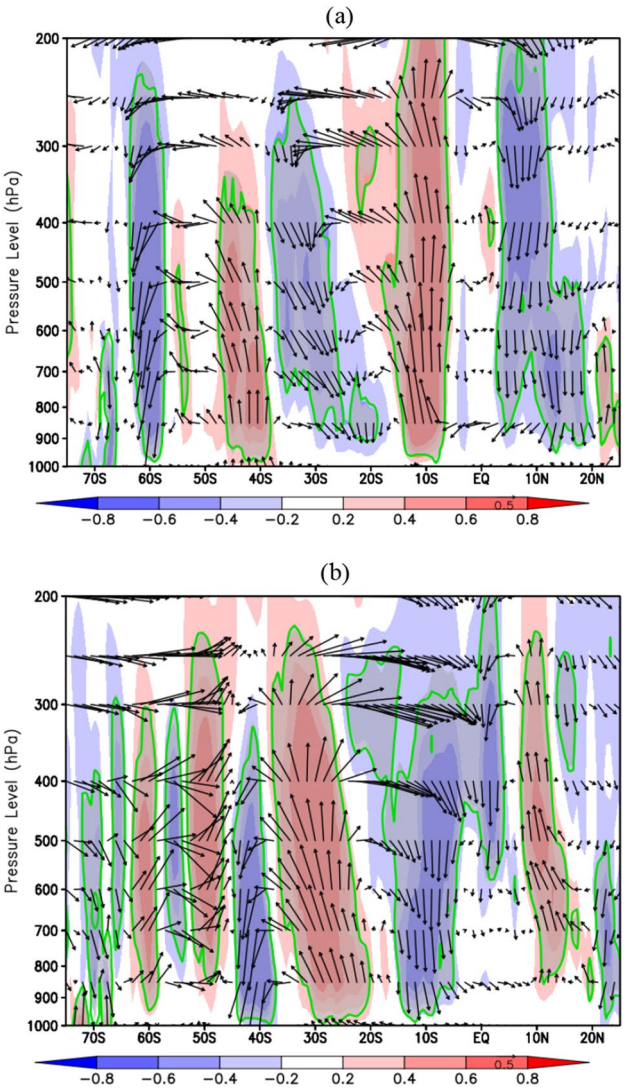

Fig. 5 The composites difference of meridional circulation averaged over the Indian Ocean longitudinal belt of 55° E–85° E, for high and low phases of EOF1/EOF3 corresponding to **a** PC1, **b** PC3 time series of AMJ SIE in the Indian Ocean sector. The shaded plot is the vertical velocity anomaly (unit: Pa/s, scaled by − 0.01) and superimposed by the vectors of meridional component wind (unit: ms^{-1}) and vertical velocity anomalies. The shaded area in grey and solid lines in green are statistically significant at $p < 0.05$

reflected in the tropics. Figure 5 illustrates the composite difference of meridional circulation corresponding to the PC1 (Fig. 5a) and PC3 (Fig. 5b) time series of AMJ SIE in the Indian Ocean sector averaged over a longitudinal belt of the Indian Ocean (55° E to 85° E) from 1000 to 200 hPa. The positive and negative vertical velocities anomalies represent the ascending and descending airflows (shaded in red/blue). During the low ice phase years of the PC1 time series of EOF1, the Polar cell in Fig. 5a is less active with lessened vertical motion from 80° S to 70° S. While, descending and ascending branch of the Ferrel cell is about 30° S and 60° S.

As for the Hadley cell, the main ascending branch is about 10° N and descending branch is around 10° S to 15° S. This is consistent with the features of the geopotential height anomaly at 250 hPa shown in Fig. 2a. The intense geopotential anomaly from 60° S to 90° S, indicates weaker subsidence in the polar region due to the weaker descent of the Polar cell. While depressed geopotential anomaly features from 55° S to 40° S indicate a weaker descending branch of the Ferrel and Hadley cells. In addition, intense anticyclonic circulation features were identified at high latitudes in the composite of zonal wind and streamline anomalies at 250 hPa (Fig. 4a), showing reduced surface subsidence or weakening of the Polar cell during the low ice phase years. The weakening of the Hadley cell and weakened upward anomalies indicated less convection activity over the latitude at about 10° N to 15° N and hence contributed to less precipitation over the region during these phase years. In contrast, the opposite features are shown in Fig. 5b. They illustrated the stronger ascending and descending airflow of the Polar, Ferrel, and Hadley cells during the high ice phase years of the PC3 time series of EOF3. This is consistent with Figs. 2b and 4b. From 60° S to 90° S, the geopotential is depressed, indicating strong subsidence in the polar region due to the stronger descent of the Polar cell. This can also be seen at the surface with the stronger outflow of cold air from the plateau during the high ice phase years. Also, at about 30° S to 40° S, the positive geopotential value (Fig. 2b) is associated with the stronger descending branch of the Ferrel and Hadley cells. According to Kim et al. (2015), the intensification of the Ferrel cell induces the dipole to mean sea level difference pattern between middle and high latitudes. Our previous study also discusses these features (Fig. 8a in Azhar et al. 2020). Furthermore, an intense cyclonic circulation identified at 70° S seen in Fig. 4b also manifests the intensification of surface subsidence/strengthening of the Polar cell during these phase years. The strengthening of the Hadley cell and strong upward circulation anomalies indicate more convective activity over the latitudes of the Indian region, as noted by a previous study (Dima et al. 2003), contributing to more precipitation. Therefore, during the high (low) ice phase year, the features discussed above indicate the strengthening (weakening) of Polar, Ferrel and Hadley cells. Furthermore, Fig. 5 also clearly shows the propagation of the meridional wave train from polar towards the tropics and vice versa, alternating of descending and ascending motion during the high and low ice phase years. Thus, what the composite analysis point to is that, even though EOF1 and EOF3 appear as distinct modes of sea ice variability in the Indian Ocean sector, high and low ice phases years of both the modes have similar responses in geopotential height, wave activity flux, zonal winds and meridional circulation.

This is consistent with the spatial pattern of the composite difference of OLR anomalies corresponding to the

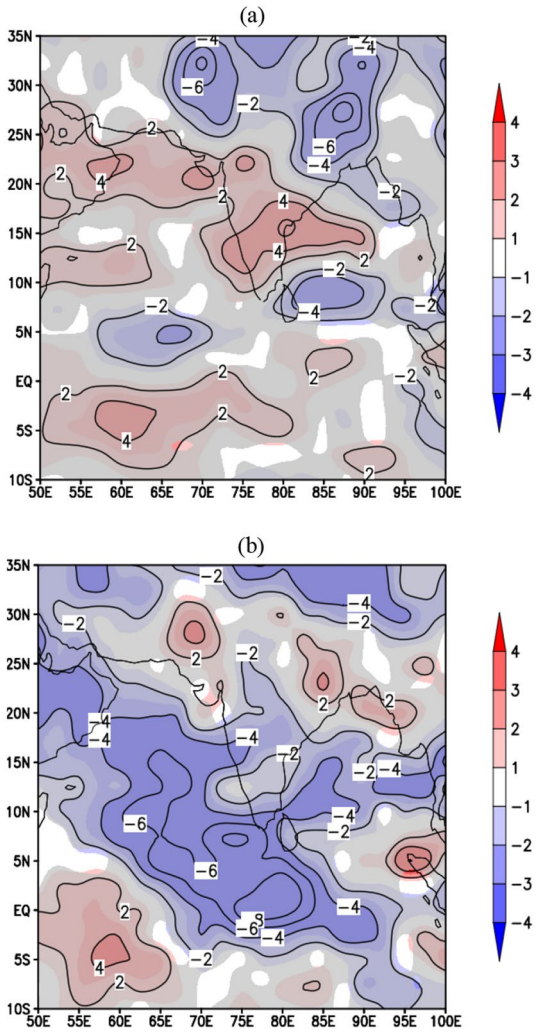

Fig. 6 The composites difference of OLR anomalies (unit: W/m$^{2)}$ for high and low phases of EOF1/EOF3 corresponding to **a** PC1, **b** PC3 time series of AMJ SIE in the Indian Ocean sector during Indian summer monsoon rainfall. The shaded area in grey is statistically significant at $p < 0.05$

PC1 (Fig. 6a) and PC3 (Fig. 6b) time series of AMJ SIE in the Indian Ocean sector during the Indian summer monsoon rainfall, shown in Fig. 6. Figure 6a shows positive OLR anomalies (reduced convection activity) over the entire India, Arabian Sea, and the western Indian Ocean, while positive OLR anomalies are seen over the north India region. This feature implies that there is less cloud formation and precipitation during the low ice phase years of the PC1 time series of EOF1 (Fig. 7a). Figure 6b shows negative OLR anomalies (enhanced convection activity) in the entire Indian region, the Arabian Sea and the Bengal Sea, while positive OLR anomalies (suppressed convection activity) are seen over the western Indian Ocean, north India, eastern India and northeast India. Consequently, the formation of clouds and precipitation increases during

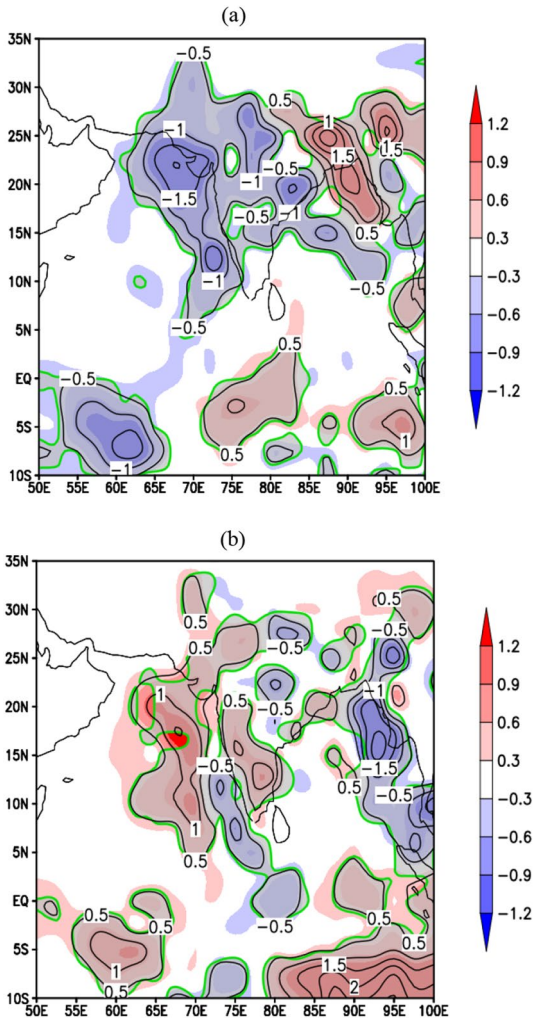

Fig. 7 The composite difference of precipitation anomalies (unit: mm/year) for high and low phases of EOF1/EOF3 corresponding to **a** PC1, **b** PC3 time series of AMJ SIE in the Indian Ocean sector during Indian summer monsoon rainfall. The shaded area in grey and solid lines in green are statistically significant at $p < 0.05$

the high ice phase years of the PC3 time series of EOF3 (Fig. 7b).

The spatial features of the composite difference of the precipitation anomalies corresponding to the PC1 (Fig. 7a) and PC3 (Fig. 7b) time series of AMJ SIE in the Indian Ocean sector shown in Fig. 7 further support this. During the low ice phase years of the PC1 time series of EOF1, negative precipitation anomalies are observed over India, the eastern Arabian Sea, and some parts of the Bengal Sea (Fig. 7a). Opposite features are seen in Fig. 7b. Positive precipitation anomalies are observed over Peninsular India, east of the Arabian Sea, near the India region, which extended to the west-north of India during the high ice phase years of the PC3 time series of EOF3. As shown in our prior study (Azhar et al. 2020, Figs. 10a, b), significant divergence anomalies were located over the Arabian Sea and west of Peninsular India at 200 hPa, with the convergence anomalies at 850 hPa. However, the location of the rainfall pattern might not be exactly similar to OLR because rainfall is controlled by other factors such as topography.

Based on the analysis above, it is evident that the relationship between SIE in the Indian Ocean sector and Indian summer monsoon rainfall is due to the meridional wave trains in the lower and upper troposphere along the Indian Ocean. These meridional wave trains affect the variabilities of the jet streams, including the variability of the wind circulation at the lower and upper levels, thereby affecting the strength of the three cells (Polar cell, Ferrel cell, and Hadley cell). In succession, the convective activity over the Indian region is affected, thus influencing the variability of the Indian summer monsoon rainfall over the Indian region. The aforementioned anomalous meridional zonal wave train pattern and the meridional circulation signify the transport of signals from the polar region towards the tropics or vice versa. Furthermore, the positive trends of the Antarctic SIE had an impact on the change in atmospheric circulation and spatial variability of global trends in surface temperature (Comiso et al. 2017; Simmonds et al. 2021), which consequently affected the strength and location of the Hadley cell (Hudson et al. 2001) as well as surface wind distribution and vertical integration of atmospheric structure (Simmonds et al. 2021). However, the implications of the positive trends are experienced differently by different sectors. It is because each Antarctic region's sector unique characteristics and natural variability influenced by its geographical location (Weeks, 2010).

4 CIMP5 models simulation

This section examines how well the CMIP5 models are able to capture the observed spatial pattern of teleconnections between SIE and the Indian summer monsoon. The high and low ice phase years of each model were categorized based on greater than 1 (less than 1) standard deviation of the normalization of SIE in the Indian Ocean sector derived from the individual models. It is noted that most of the CMIP5 models were diagnosing decreases in Antarctic SIE (over 1979–2013), while the observations were exhibiting the opposite behaviour. However, a previous study (Shu et al. 2012, 2015), shows positive trends in autumn for all sectors, including the Indian Ocean sector except Bellingshausen and Amundsen seas. Furthermore, there are few models that can adequately reproduce the seasonal cycle of Antarctic SIE (Turner et al. 2013; Shu et al. 2015).

The spatial correlation of zonal wind anomalies between the ERA-Interim reanalysis and CMIP5 models for the high and low ice phase years is determined to assess the ability

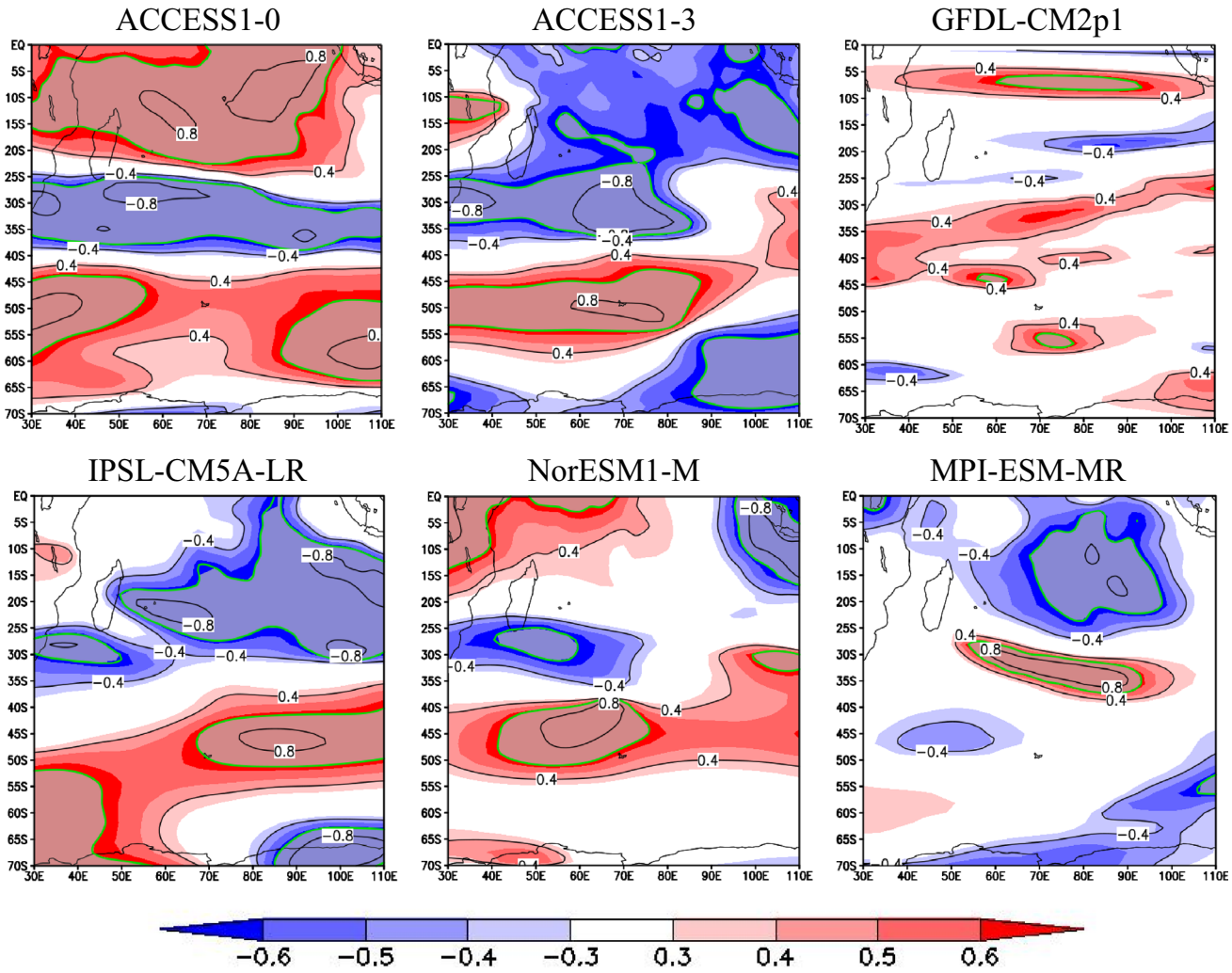

Fig. 8 The correlation of zonal wind between the ERA-Interim reanalysis and CMIP5 models during MJJ for high ice phase years at level 250 hPa. The shaded area in grey and solid lines in green are statistically significant at $p < 0.05$

of the CMIP5 model to simulate the teleconnection pattern (Figs. 8 and 9). The correlation coefficient from each model is favourably linked with the ERA-Interim reanalysis, as indicated by the shaded red area, and the opposite is true for the blue shaded area. The anomaly correlation coefficient average in the study area is computed to characterize better the representation of the amplitude of the teleconnection pattern in CMIP5 models and ERA-Interim (Figs. 10a, b). The models NorESM1-M, MPI-ESM-MR, IPSL-CM5A-LR and ACCESS 1.3 reveal a positive correlation (0.50–0.62) during the high ice phase years (Fig. 10a). The IPSL-CM5A-LR model shows a highest positive correlation (0.62) for the low ice phase years, followed by MPI-ESM-MR and NorESM1-M model. While others show a negative correlation (Fig. 9b). In general, moderate to higher anomaly correlation coefficient averages from NorESM1-M, MPI-ESM-MR, IPSL-CM5A-LR and ACCESS 1.3 indicates that they display relatively similar zonal wind anomalies pattern during the high ice phase years. At the same time, only the IPSL-CM5A-LR model displays a relatively comparable zonal wind anomaly pattern during the low ice phase years.

The analysis in the previous sections shows that the atmospheric circulation anomalies over the Indian Ocean as well as the convective activity over the Indian region changed during the high and low ice phase years. A similar analysis was carried out to identify if the selected CMIP5 models could capture the teleconnection between the SIE in the Indian Ocean sector and Indian summer monsoon rainfall. The correlation analysis shows that the SIE of the NORESMI-M model during AMJ was the most significantly correlated with the PC2 time series of Indian summer monsoon rainfall from 1979 to 2012 (33 years), with a correlation coefficient of 0.32 ($p < 0.1$). On the other hand, the SIE of the IPSL-CM5A-LR model gives an opposite

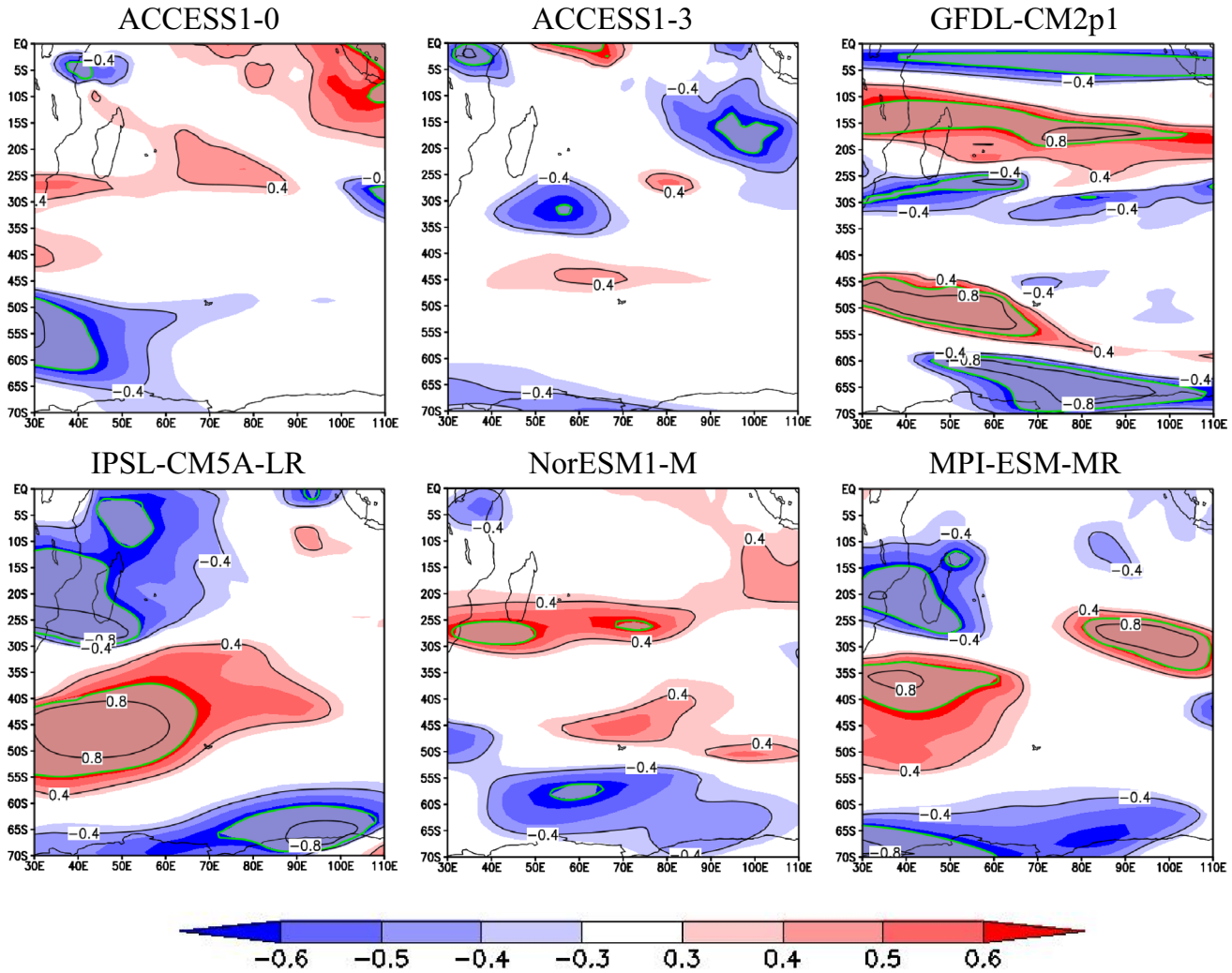

Fig. 9 The correlation of zonal wind anomalies between the ERA- Interim reanalysis and CMIP5 models during MJJ for low ice phase years at level 250 hPa. The shaded area in grey and solid lines in green are statistically significant at $p < 0.05$

relationship with the PC2 time series of Indian summer monsoon rainfall, with a correlation coefficient of − 0.30 ($p < 0.1$). The other models (ACCESS 1.0, ACCESS 1.3, MPI-ESM-MR and GFDL–CM2.1) show an insignificant relationship with the Indian summer monsoon rainfall in all composite months. The summary of the correlation coefficient between the SIE (CMIP5 models and HadISST) with the precipitation is tabulated at Table 4. The spatial correlation between SIE of CMIP5 models and precipitation data for 33 years (Fig. 11) were analyzed. NORESMI-M models show a positive correlation on the west coast of Peninsular India, while IPSL-CM5A-LR models show a negative correlation in the different parts in Indian region. Thus, the two models (NORESMI-M and IPSL-CM5A-LR) that show a significant relationship with the Indian summer monsoon rainfall will be used for further analysis.

Figure 12 illustrates a similar parameter as in Fig. 2 for two model simulations, NORESMI-M and IPSL-CM5A-LR. The NORESMI-M model produces a slightly similar pattern to the reanalysis result (Fig. 2b) and a better result than the IPSL-CM5A-LR model. The NORESMI-M model shows the dipole pattern of geopotential height (shaded) along the Indian Ocean. However, the position of the positive value in this model is more westward and much lower than the reanalysis result. As for the wave-activity flux difference, there are no particular patterns over the polar and mid-latitudes. However, propagation of wave activity flux towards the equator at about 25° S in the western part of the Indian Ocean near Madagascar can be noted. Nevertheless, the NORESMI-M model shows a strong equatorward flow of wave-activity flux along the longitudes at about 10° S. For the IPSL-CM5A-LR model, no dipole pattern of geopotential height is seen along the Indian Ocean.

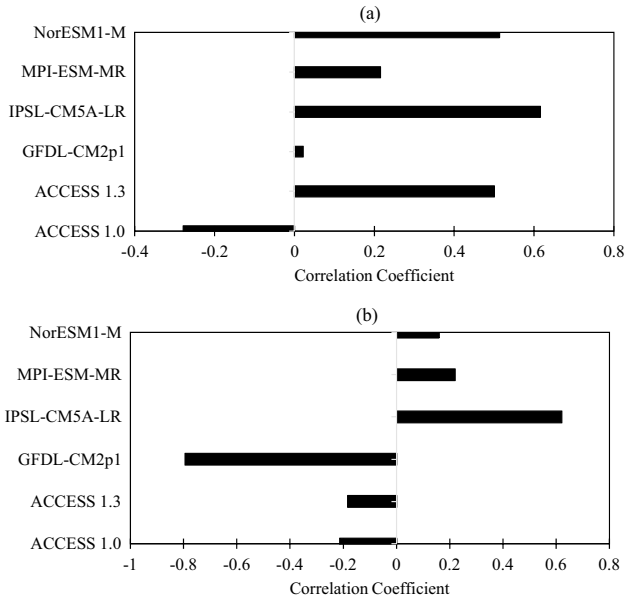

Fig. 10 The correlation coefficient of zonal wind anomalies between the ERA- Interim reanalysis and CMIP5 models during MJJ for **a** the high ice phase years and **b** the low ice phase years from the study area (lon: 55° E–85° E, lat: 30° S–60° S) at 250 hPa

Table 4 Summary of correlation coefficient of selected CMIP5 models and HadISST dataset

SIE in the Indian Ocean sector (AMJ) and PC2 of Precipitation (GPCP) during Indian summer monsoon rainfall		
CMIP5 models (1979–2012):	correlation coefficient (r)	p value
NorESM1-M	0.32	0.069**
IPSL–CM54-LR	− 0.30	0.089**
HadISST datasets (1979–2013):		
PC1	− 0.49	0.0028*
PC3	0.40	0.0173*

p value statistically at *$p < 0.05$ and **$p < 0.1$

As indicated by the reanalysis results, the variability of wind at the lower and upper levels is an important factor in the teleconnection feature between the SIE in the Indian Ocean sector and Indian summer monsoon rainfall. The vertical profile of the composite difference of the zonal wind average for the NorESM1-M and IPSL–CM5A-LR models is shown in Fig. 13. Both models were able to generate the features of polar and subtropical jets at levels of pressure ranging from 200 to 400 hPa. As compared with reanalysis results, the IPSL–CM5A-LR model produce nearly similar features in 3b, especially polar and subtropical jets. However, the difference in anomaly values for both models is relatively small, indicating the small impact on the polar and subtropical jets in both phases. Figure 14 shows the spatial pattern of the composite difference of zonal wind anomalies superimposed with wind anomalies at 250 hPa for both model simulations. Both models successfully simulate a pattern along the Indian Ocean. The features of the zonal and wind circulation anomalies produced by IPSL–CM5A-LR model are nearly similar to the reanalysis results (Fig. 4b). However, the position of the zonal wind anomaly pattern is more southward, and the anticyclone circulation can be only seen at about 75° S–55° S of the western Indian Ocean (Fig. 14b). In contrast, the NorESM1-M model shows the opposite pattern with the reanalysis.

The composite difference of the meridional circulation produced by the model simulation is illustrated in Fig. 15 for NorESM1-M and IPSL–CM5A-LR models. The results produced by both models show no apparent features compared to the reanalysis results, especially the IPSL–CM5A-LR model. The NorESM1-M model produces somewhat similar patterns with Fig. 5b at about 10° N for both phases. The anomalous rising motion can only be seen at about 10° S and 10° N, indicating the enhancement of convective activity during the high ice phase years. Similar features as in the reanalysis can also be seen with the anomalous rising motion at about 70° S and anomalous sinking motion at about 15° N. Contrary to the reanalysis results, at about 30° S an anomalous descending air is noted. Overall, the features of rising (sinking) motion at about 10° N produced by the NorESM1-M model during high (low) ice phases years indicate enhanced (depressed) convective activity.

The spatial pattern of the composite difference of OLR anomalies simulated by the models is shown in Fig. 16. The features of the OLR anomaly of the NorESMI-M model show slightly comparable results with the reanalysis (Fig. 6b), especially during the low ice phase years, even though the location of the shaded area is slightly different (Fig. 16a). Positive OLR anomalies are seen over the southern Peninsular India and some parts of north-eastern India. While the negative OLR anomalies are seen over the northwest of India, the central part of India and the Arabian Sea. The IPSL-CM5A-LR model shows an opposite outcome to the reanalysis for both phases. Positive OLR anomalies are seen over the entire India region, including the Arabian Sea and Bengal Sea (Fig. 16b).

Overall, both models are capable of producing certain features. For example, the IPSL-CM5A-LR model is capable of producing characteristics (polar jet, subtropical jet, zonal wind and wind circulation anomalies) that are almost identical to the results of the reanalysis for the high and low ice phases. While, the NorESM1-M model was able to capture features of meridional circulation, convective activity and OLR, especially during the low ice phase years. The results shown by both reanalysis and numerical models are limited to the period 1979–2013, and the teleconnection features may be slightly different and vary if the period is

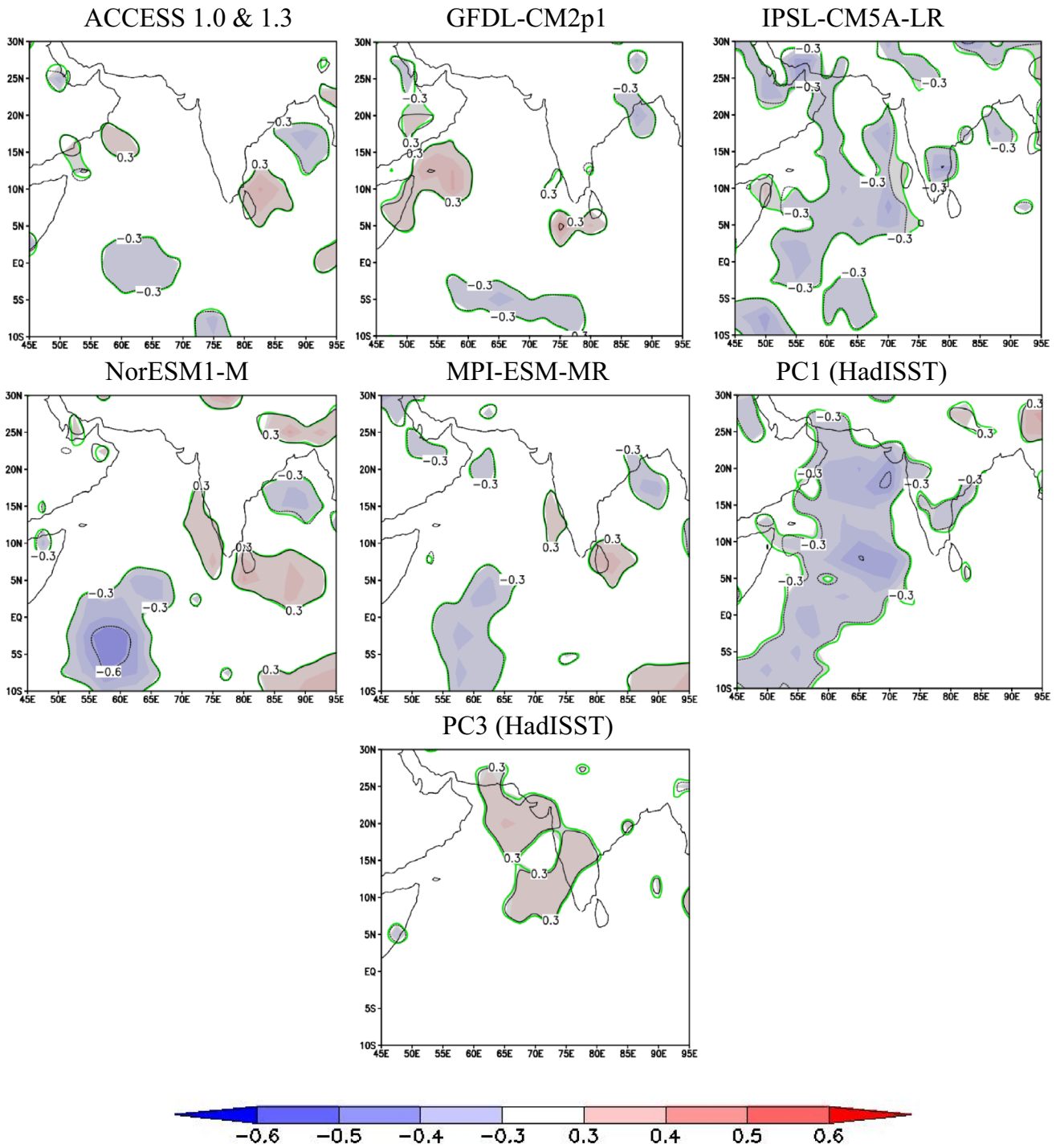

Fig. 11 The spatial correlation between the sea ice (CMIP5 models and HadISST dataset) with Indian summer monsoon rainfall (GPCP). The shaded area in grey and solid lines in green are statistically significant at $p < 0.05$

extended. As documented in a recent study by Simmonds et al. (2021), the annual Antarctic SIE increased up to 2014 and then remarkably decreased until 2017, and in 2020 it increased back to almost its long term average value. Their results stated that the significant changes in the distribution of climatological SLPs, vertical shear of the horizontal wind, and static stability are the major factors in the changes in baroclinicity over the polar regions. However, as mentioned above, different sectors of Antarctica may experience different changes due to its geophysical factors. For example, the authors reported strong mean baroclinicity just north of the Antarctic continent in all seasons, particularly in the Indian

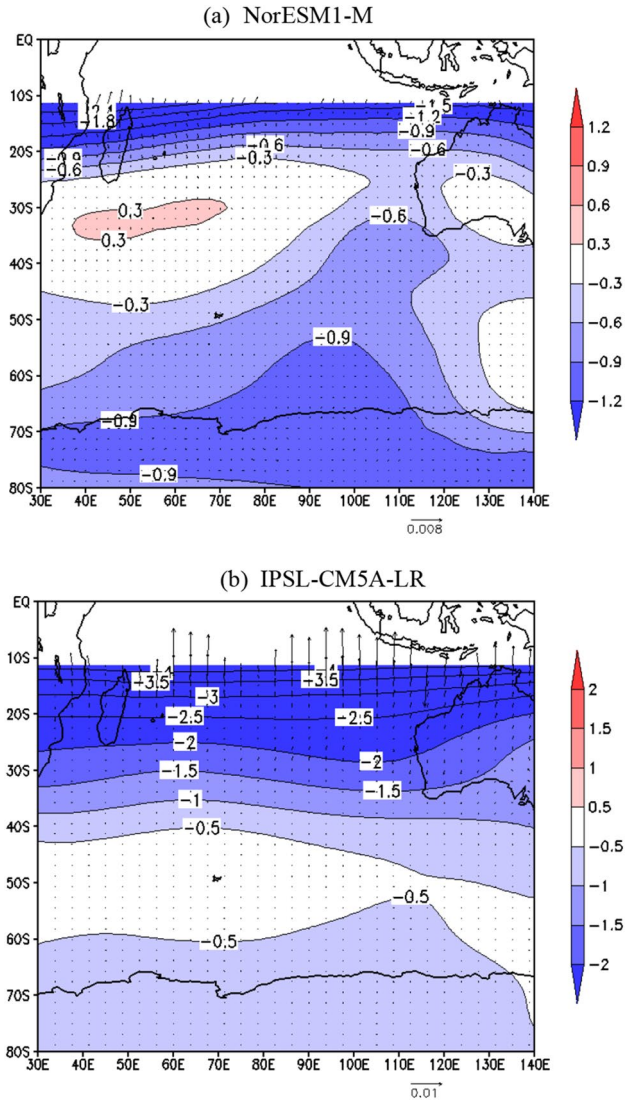

Fig. 12 The regressed anomalous contour of geopotential height anomalies (shaded, unit: m) for 35 years superimposed with the composite difference of high and low ice phase years of wave–activity flux (vector, unit: m^2s^{-2}) during MJJ at 250 hPa for the NorESM1-M and IPSL–CM5A-LR models

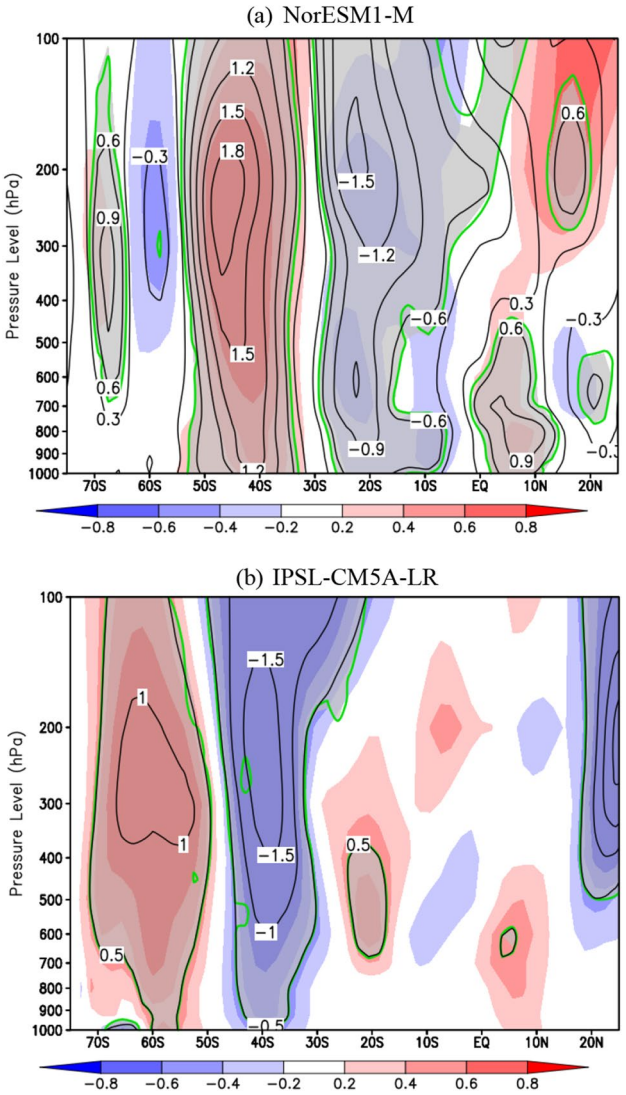

Fig. 13 The vertical profile of composite difference of high and low ice phase years of zonal wind average (unit: ms^{-1}, averaged over 55° E–85° E) for **a** NorESM1-M and **b** IPSL–CM5A-LR models. The shaded area in grey and solid lines in green are statistically significant at $p < 0.05$

Ocean sector and to the south of Australia and New Zealand. Therefore, it is uncertain how the pattern of the teleconnections would change if the sea ice trends and circulation for the period had been considered. Furthermore, the bias of the models can be treated by considering several aspects, such as internal variability, dynamic and thermodynamic contributions. Hence, it is crucial to understand the ability of these models to recreate observed sea ice metrics and processes (Bracegirdle et al. 2019).

5 Summary and conclusion

Azhar et al. (2020) demonstrated the positive links between SIE during AMJ and the variability of summer monsoon rainfall over the Peninsular India region through the variability of Mascarene high. The strengthening (weakening) of Mascarene high during high (low) ice phase years leads to increased (decreased) cross-equatorial flows, which in turn contributes more (less) than average Indian summer monsoon rainfall.

The present study investigated the possible mechanisms by which SIE in the Indian Ocean sector affects Indian summer monsoon rainfall in terms of atmospheric circulations.

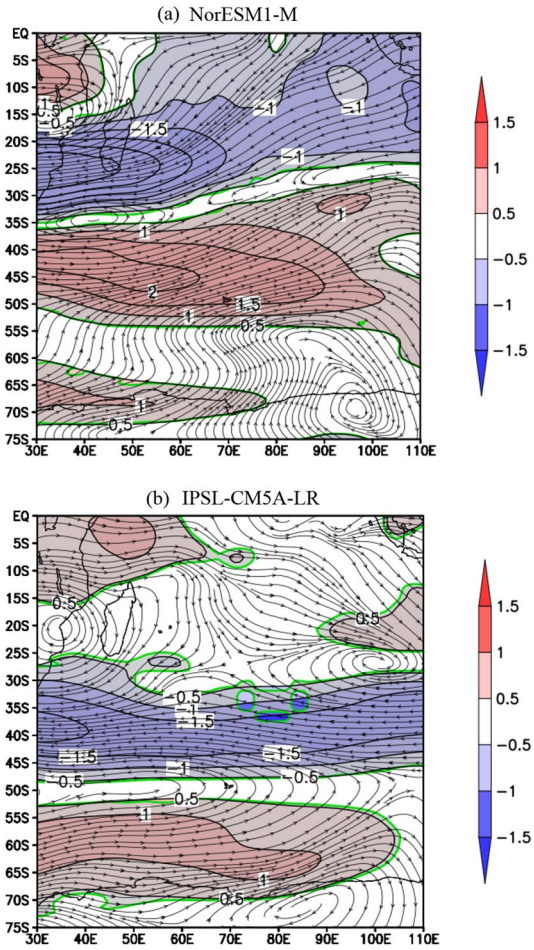

Fig. 14 The composite difference of high and low ice phase years of zonal wind anomaly (shaded) superimposed with wind anomaly (streamlines) at 250 hPa (unit: ms^{-1}) for **a** NorESM1-M and **b** IPSL–CM5A-LR models. The shaded area in grey and solid lines in green are statistically significant at $p < 0.05$

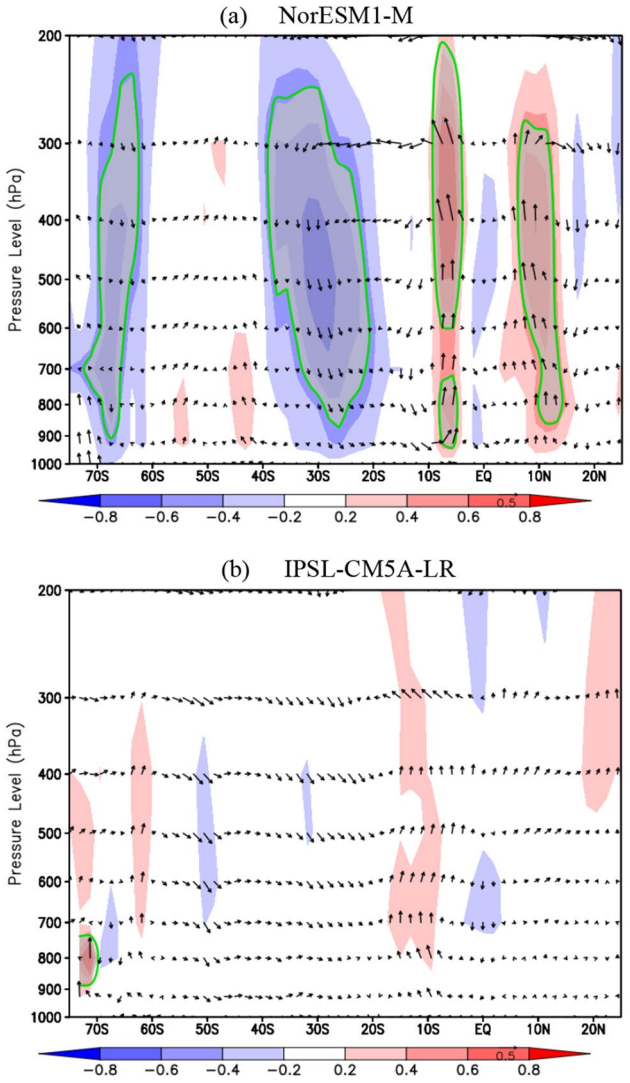

Fig. 15 The composites difference of high and low ice phase years of anomalous meridional circulation averaged over the Indian Ocean longitudinal belt of 55° E–85° E for the NorESM1-M and IPSL–CM5A-LR models. The shaded plot is the vertical velocity (unit: Pa/s, scaled by − 0.01) and superimposed by the vectors of meridional component wind (unit: ms^{-1}) and vertical velocity anomalies. The shaded area in grey and solid lines in green are statistically significant at $p < 0.05$

The empirical orthogonal function (EOF) and correlation analysis show that the first and third modes of principal component (PC1 and PC3) of SIE in the Indian Ocean sector during April–May-June (AMJ) are significantly correlated with the second mode of principal component (PC2) of Indian summer monsoon rainfall. Based on the reanalysis results, an anomalous meridional wave train appears at the lower and upper troposphere along the Indian Ocean for both principal component modes, propagating from the polar region towards the middle latitude and the tropics. In conjunction with that, changes in jets strength and the wind circulation at upper and lower levels in the middle latitude and the tropics were observed. In contrast, the subtropical jet shows not much difference between both phases. During the high ice phase, an intense anticyclonic and cyclonic wind anomaly over the southern Indian Ocean and the central Indian Ocean at 250 hPa were noted. These features imply more substantial surface convergence and divergence during the high ice phase years. The composite anomaly of meridional circulation and vertical velocity during the high ice phase years illustrate meridionally propagating waves trains, leading to strengthening the Polar, Ferrel, and Hadley cells. In addition, strengthening of cross-equatorial flow due to the stronger (weakening) Mascarene high is noted during the high sea ice phase. Subsequently, enhanced Hadley cell, the more vigorous convective activity over the India region hence increases Indian summer monsoon rainfall. Opposite features were observed for the low ice phase years with a weaker polar front jet. Weak divergence and convergence

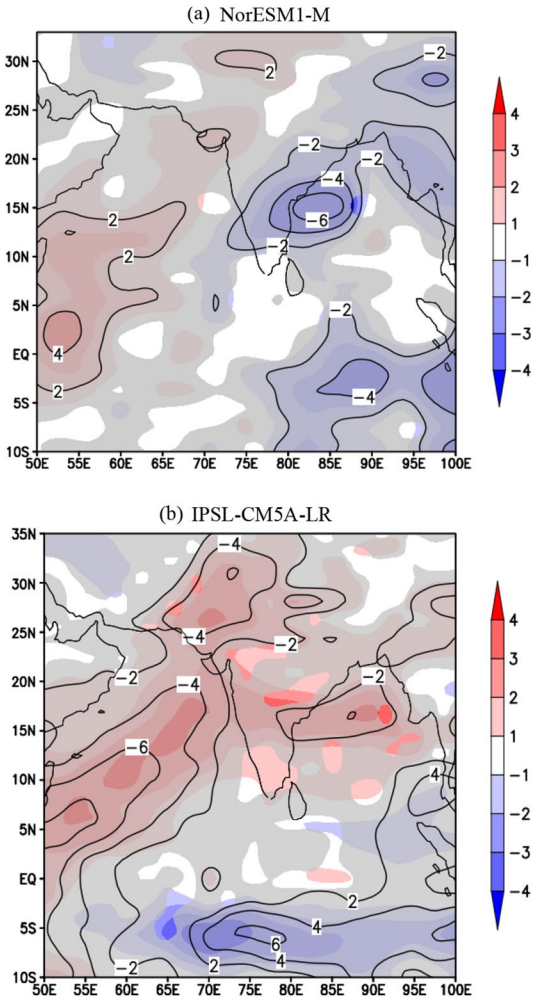

Fig. 16 The composite difference of high and low ice phase years of OLR anomaly (unit: W/m^2) for the **a** NorESM1-M & **b** IPSL–CM5A-LR models during Indian summer monsoon rainfall. The shaded area in grey is statistically significant at $p < 0.05$

anomaly at the upper level are associated with weak convergence and divergence at lower levels and weakening of the Polar, Ferrel, and Hadley cells. Consequently, low convective activity and decreased cloud formation as well as the precipitation over the India region. The proposed mechanism of teleconnection during high ice phase years is summarized in Fig. 17.

Evaluation of selected CMIP5 models has been performed by comparing the spatial pattern of teleconnection between SIE and the Indian summer monsoon simulated by the models with the ERA-Interim reanalysis. Analysis of the correlation coefficient of zonal wind anomaly between the reanalysis and CMIP5 models shows that more than half of the selected models display a significant positive correlation during the high ice phase. Furthermore, NorESM1-M and IPSL–CM5A-LR could capture certain atmospheric circulation features similar to the reanalysis. For example, the NorESM1-M model captured the teleconnection features in meridional circulation, convective activity and OLR, especially during the low ice phase years. However, the location of the meridional circulation cell is shifted slightly more northward than the reanalysis results. At the same time, the IPSL-CM5A-LR model reproduced similar features of polar jet, subtropical jet, zonal wind and wind circulation anomalies with the reanalysis in both sea ice phases. The difference in the results between the simulations and observations may be due to the poor representation of natural climate variability (Stroeve et al. 2012). In summary, NorESM1-M and IPSL–CM5A-LR could be used to examine how the linkages between the sea ice variability and the Indian summer monsoon might change in the future.

In conclusion, the propagation of the meridional wave train along the Indian Ocean links the change in the SIE in the Indian Ocean sector of the Southern Ocean to the variability of Indian summer monsoon rainfall. The jets' variabilities and wind circulation at upper and lower levels are

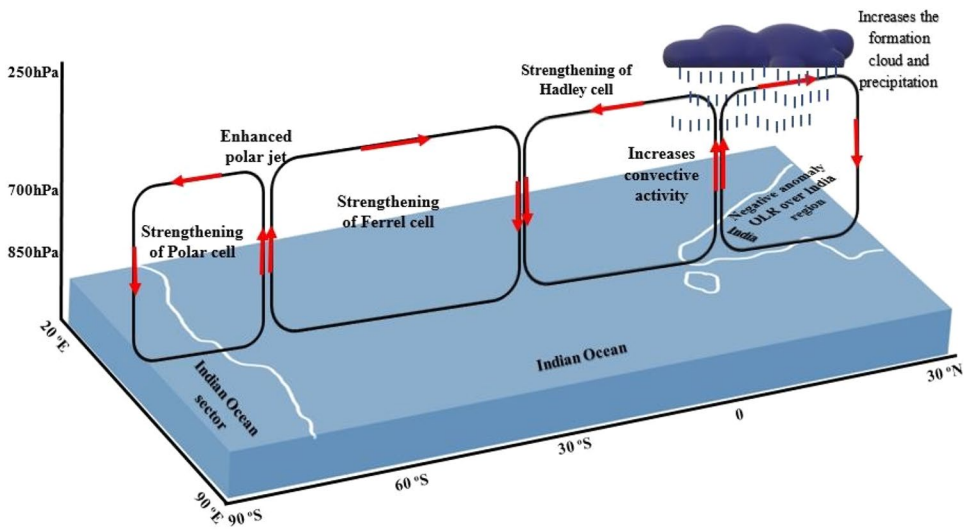

Fig. 17 The schematic diagram of the mechanism of teleconnection during high ice phase years

the key teleconnection mechanisms. The study suggests an explanation for teleconnection mechanisms that connect the polar region to the tropics in terms of atmospheric circulation features. The idea proposed is limited to the SIE in the Indian Ocean sector during AMJ. The air-sea interaction and global model simulation will be considered in future work.

Acknowledgements This study is funded by Fundamental Research Grant Scheme (FRGS) Project NoFP059-2019A and the Ministry of Sciences Technology and Innovation Flagship Grant: FP1213E037. It is also strongly supported by the Academic Sciences of Malaysia, Sultan Mizan Antarctic Research Foundation, Malaysian Antarctic Research Program and the Vice-Chancellor of the University Malaya. This work was also supported by the action group Tropical Antarctic Teleconnections (TATE) under Scientific Committee on Antarctic Research (SCAR). S.-J. Kim was supported by the project (PE22030) of the Korea Polar Research Institute. Also, many thanks to everyone who contributed directly or indirectly to the paper.

Author contributions All authors contributed to the study conceptions. Material preparation and data collection analysis were performed by SSAA. The first draft of the manuscript was written by SSAA, and all authors commented on all the versions. All authors read and approved the final manuscript.

Fundings This work was supported by Fundamental Research Grant Scheme (FRGS: FP059-2019A), the Ministry of Sciences Technology and Innovation Flagship Grant (FP1213E03) and Academic Sciences of Malaysia, Sultan Mizan Antarctic Research Foundation, Malaysian Antarctic Research Program. Seong-Joong Kim was supported by the project (PE22030) of the Korea Polar Research Institute. Fundamental Research Funds for the Central Universities; Kementerian Sains, Teknologi dan Inovasi.

Data Availability The datasets used in this study are available in the ERA-Interim(https://apps.ecmwf.int/datasets/data/interim-full-daily/levtype=sfc/), Met Office Hadley Centre Global Sea Ice and Sea Surface Temperature (https://www.metoffice.gov.uk/hadobs/hadisst/data/download.html), Global Precipitation Climatology Project(https://psl.noaa.gov/data/gridded/data.gpcp.html), National Center for Atmospheric Research (https://climatedataguide.ucar.edu/climate-data/outgoing-longwave-radiation-olr-avhrr) and CMIP5 (https://esgf-node.llnl.gov/projects/esgf-llnl/).

Declarations

Conflict of interest The authors have no relevant financial or non-financial interests to disclose.

References

Azhar SS, Chenoli SN, Samah AA, Kim SJ (2020) The linkage between Antarctic sea ice extent and Indian summer monsoon rainfall. Polar Sci 25(100537):1–10. https://doi.org/10.1016/j.polar.2020.100537

Bajish CC, Jena B, Anilkumar N (2021) Is the Indian monsoon rainfall linked to the Southern Ocean sea ice conditions? Weather Clim Extrem 34(100377):1–8

Bi D, Dix M, Marsland SJ, O'Farrell S, Rashid HA, Uotila P, Hirst AC, Kowalczyk E, Golebiewski M, Sullivan A, Yan H, Hanna N, Franklin C, Sun Z, Vohralik P, Watterson I, Zhou X, Fiedler R, Collier M, Ma Y, Noonan J, Stevens L, Uhe P, Zhu H, Hill R, Harris C, Griffies S, Puri K (2013) The ACCESS coupled model: description, control climate and preliminary validation. Aust Met Oceanog J 63:41–64

Blackport R, Screen JA (2020) Insignificant effect of Arctic amplification on the amplitude of midlatitude atmospheric waves. Sci Adv 6(8):1–9. https://doi.org/10.1126/sciadv.aay2880

Bracegirdle T, Holmes C, Holland P (2019) Compensating biases and a noteworthy success in the CMIP5 representation of Antarctic sea ice processes. Geophys Res Lett 46:4299–4307. https://doi.org/10.1029/2018GL081796

Bromwich DH, Chen B, Hines KM (1998) Global atmospheric impacts induced by year-round open water adjacent to Antarctica. J Geophys Res 103(D10):11173–11189

Carvalho LMV, Jones C, Tercio A, Ambrizzi T (2005) Opposite phases of the Antarctic Oscillation and relationships with intraseasonal to interannual activity in the tropics during the Austral Summer. J Clim 18:702–718. https://doi.org/10.1175/JCLI-3284.1

Chatterjee S, Ravichandran M, Murukesh N et al (2021) A possible relation between Arctic sea ice and late season Indian Summer Monsoon Rainfall extremes. Npj Clim Atmos Sci 4(36):1–6. https://doi.org/10.1038/s41612-021-00191-w

Chen C, Guan Z, Jiao M, Hu P (2019) Anomalous circulation patterns in association with summertime regional daily precipitation extremes over Northeast China. Adv Meteorol 2019(5085897):1–9. https://doi.org/10.1155/2019/5085897

Clift P, Plumb R (2008) The Asian Monsoon: causes, history and effects. Cambridge University Press, Cambridge. https://doi.org/10.1017/CB09780511535833

Cohen J, Screen JA, Furtado JC et al (2014) Recent Arctic amplification and extreme mid-latitude weather. Nat Geosci 7(9):627–637. https://doi.org/10.1038/ngeo2234

Collins WJ, Bellouin N, Doutriaux-Boucher M, Gedney N, Hinton T, Jones CD, Liddicoat S, Martin G, O'Connor F, Rae J, Senior C, Totterdell I, Woodward S, Reichler T, Kim J (2008) Evaluation of the HadGEM2 model. Met Office Hadley Centre Technical Note no. HCTN 74, available from Met Office, FitzRoy Road, Exeter EX1 3PB. http://www.metoffice.gov.uk/publications/HCTN/index.html

Comiso JC, Gersten RA, Stock LV, Turner J, Perez GJ, Cho K (2017) Positive trend in the Antarctic Sea Ice Cover and associated changes in surface temperature. J Clim 30(6):2251–2267. https://doi.org/10.1175/JCLI-D-16-0408.1

Dima IM, Wallace JM (2003) On the seasonality of the Hadley cell. J Atmos Sci 60:1522–1527

Dugam SS, Kakade SB (2004) Antarctica sea-ice and monsoon variability. Indian J Radio Space Phys 33:306–309

Gadgil S (2006) The Indian Monsoon. GDP Agric Econ Polit Wkly 41(47):4887–4895

Guo D, Gao Y, Bethke I, Gong D, Johannessen OM, Wang H (2014) Mechanism on how the spring Arctic sea ice impacts the East Asian summer monsoon. Theor Appl Climatol 115(1-2):107–119

He J, Lin H, Wu Z (2011) Another look at influences of the Madden–Julian Oscillation on the wintertime East Asian Weather. J Geophys Res 116(D03109):1–18. https://doi.org/10.1029/2010JD014787

Hines KM, Bromwich DH (2002). A pole to pole west Pacific atmospheric teleconnection during August. J Geophys Res 107 (D18): ACL 8-1-ACL 8-20. https://doi.org/10.1029/2001JD001335.

Holmes CR, Holland PR, Bracegirdle TJ (2019) Compensating biases and a noteworthy success in the CMIP5 representation of Antarctic sea ice processes. Geophys Res Lett. https://doi.org/10.1029/2018GL081796

Hoskins BJ, Ambrizzi T (1993) Rossby wave propagation on a realistic longitudinally varying flow. J Atmos Sci 50(12):1661–1671.

https://doi.org/10.1175/15200469(2003)060%3c1522:OTSOTH%3e2.0.CO;2
Hu YY, Fu Q (2007) Observed poleward expansion of the Hadley circulation since 1979. Atmos Chem Phys 7:5229–5236. https://doi.org/10.5194/acp-7-5229-2007
Hu Y, Huang H, Zhou C (2018) Widening and weakening of the Hadley circulation under global warming. Sci Bull 63:640–644
Hudson DA, Hewitson BC (2001) The atmospheric response to a reduction in summer Antarctic sea-ice extent. Clim Res 16:79–99
Jin D, Guan Z, Huo L, Wang X (2017) Possible impacts of spring sea surface temperature anomalies over South Indian Ocean on summer rainfall in Guangdong-Guangxi region of China. Clim Dyn 49:3075–3090
Kim YH, Kim MK, Lau WK, Kim KM, Cho CH (2015) Possible mechanism of abrupt jump 607 in winter surface air temperature in the late 1980s over the Northern Hemisphere. J Geophys Res 608 Atmos 120(24):1–12
Lamarque JF, Bond TC, Eyring V, Granier C, Heil A, Klimont Z et al (2010) Historical (1850–2000) gridded anthropogenic and biomass burning emissions of reactive gases and aerosols: methodology and application. Atmos Chem Phys 10:7017–7039. https://doi.org/10.5194/acp-10-7017-2010
Li J, Wang JXL (2003) A modified zonal index and its physical sense. Geophys Res Lett 30(12):34–38. https://doi.org/10.1029/2003GL017441
Li X, Cai W, Meehl GA et al (2021) Tropical teleconnection impacts on Antarctic climate changes. Nat Rev Earth Environ 2:680–698. https://doi.org/10.1038/s43017-021-00204-5
Liu J, Yuan X, Rind D, Martinson DG (2002) Mechanism study of the ENSO and southern high latitude climate teleconnections. Geophys Res Lett 29(14):241–244. https://doi.org/10.1029/2002GL015143
Liu N, Zhang Z, Chen H, Lin L (2011) Western Indian Ocean SST signal and anomalous Antarctic sea-ice concentration variation. Acta Oceanol Sin 30(2):9–13. https://doi.org/10.1007/s13131-011-0100-0
Liu N, Li S (2018) Connection of Antarctic sea ice variability with China summer rainfall on the interannual timescale. American Geophysical Union
Luo X, Zhang Y (2015) The linkage between upper-level jet streams over East Asia and East Asian Winter Monsoon Variability. J Clim 28(22):9013–9028. https://doi.org/10.1175/JCLI-D-15-0160.1
Mahlstein I, Gent PR, Solomon S (2013) Historical Antarctic mean sea ice area, sea ice trends, and winds in CMIP5 simulations. J Geophys Res-Atmos 118:5105–5110
Menzel ME, Waugh D, Grise K (2019) Disconnect between Hadley cell and subtropical jet variability and response to increased CO2. Geophys Res Lett 46(12):7045–7053
Moss RH, Edmonds JA, Hibbard KA, Manning MR et al (2010) The next generation of scenarios for climate change research and assessment. Nature 463:747–756
Nguyen H, Evans A, Lucas C, Smith I, Timbal B (2013) The Hadley circulation in reanalyses: climatology, variability, and change. J Clim 26:3357–3376
Nuncio M, Yuan XJ (2015) The influence of the Indian Ocean Dipole on Antarctic Sea Ice. J Clim 28:2682–2690. https://doi.org/10.1175/JCLI-D-14-00390.1
Ogwang BA, Ongoma V, Xing L, Ogou FK (2015) Influence of mascarene high and Indian Ocean Dipole on East African extreme weather events. Geographica Pannonica 19(2):64–72
Pezza A, Durrant T, Simmonds I (2008) Southern hemisphere synoptic behavior in extreme phases of SAM, ENSO, Sea Ice Extent, and Southern Australia rainfall. J Clim 21:5566–5584
Pezza AB, Rashid HA, Simmonds I (2012) Climate links and recent extremes in Antarctic sea ice, high-latitude cyclones, Southern Annular Mode and ENSO. Clim Dyn 38:57–73
Prabhu A, Mahajan P, Khaladkar R, Bawiskar S (2009) Connection between Antarctic sea-ice extent and Indian summer monsoon rainfall. Int J Remote Sens 30(13):3485–3494. https://doi.org/10.1080/01431160802562248
Prabhu A, Kripalani RH, Preethi B, Pandithurai G (2016) Potential role of the February–March Southern Annular Mode on the Indian summer monsoon rainfall: a new perspective. Clim Dyn 47(3–4):1161–1179. https://doi.org/10.1007/s00382-015-2894-5
Prabhu A, Oh J, Kim I, Kripalani RH, Pandithurai G (2017) SMMR–SSM/I derived Greenland Sea ice variability: links with the Indian and Korean Monsoons. Clim Dyn 50(3–4):1023–1043. https://doi.org/10.1007/s00382-017-3659-0
Pritpal S (2018) Indian summer monsoon rainfall (ISMR) forecasting using time series data: a fuzzy-entropy-neuro based expert system. Geosci Front 9(4):1243–1257
Rai S, Pandey AC (2006) Antarctica sea ice variability in recent years and its relationship with Indian Ocean SST. J Indian Geophys Union 10(3):219–229
Rai S, Khare N, Pandey AC (2008) Antarctica sea ice variability and southeast Indian Ocean SST: possible relationship. Indian J Mar Sci 37(1):35–39
Rashid HA, Hirst AC, Dix M (2013) Atmospheric circulation features in the ACCESS model simulations for CMIP5: historical simulation and future projections. Aust Meteorol Oceanogr J 63:154–160
Rayner NA, Parker DE, Horton EB, Folland CK et al (2003) Global analyses of sea surface temperature, sea ice, and night marine air temperature since the late nineteenth century. J Geophys Res 108(D14):1–37. https://doi.org/10.1029/2002JD002670
Rehman SU, Khan K, Simmonds I (2019) Links between Tasmanian precipitation variability and the Indian Ocean subtropical high. Theoret Appl Climatol 138(4):1255–1267. https://doi.org/10.1007/s00704-019-02891-z
Rudeva I, Simmonds I, Crock D, Boschat G (2019) Midlatitude fronts and variability in the Southern Hemisphere Tropical Width. J Clim 32(23):8243–8260. https://doi.org/10.1175/JCLI-D-18-0782.1
Schneider DP, Okumura Y, Deser C (2012) Observed Antarctic Interannual climate variability and tropical linkages. J Clim 25:4048–4066. https://doi.org/10.1175/JCLI-D-11-00273.1
Screen JA, Bracegirdle TJ, Simmonds I (2018) Polar climate change as manifest in atmospheric circulation. Curr Clim Change Rep 4:383–395. https://doi.org/10.1007/s40641-018-0111-4
Shen H, He S, Wang H (2019) Effect of Summer Arctic Sea Ice on the Reverse August Precipitation Anomaly in Eastern China between 1998 and 2016. J Clim 32:3389–3407
Shi W, Xiao Z, Xue J (2016) Teleconnected Influence of the Boreal Winter Antarctic Oscillation on the Somali Jet: Bridging Role of Sea Surface Temperature in Southern High and Middle Latitudes. Adv Atmos Sci 33:47–57
Shu Q, Qiao F, Song Z, Wang C (2012) Sea ice trends in the Antarctic and their relationship to surface air temperature during 1979–2009. Clim Dyn 38(11–12):2355–2363
Shu Q, Song Z, Qiao F (2015) Assessment of sea ice simulations in the CMIP5 models. Cryosphere 9(1):399–409
Simmonds I (2015) Comparing and contrasting the behaviour of Arctic and Antarctic sea ice over the 35-year period 1979–2013. Ann Glaciol 56(69):18–28. https://doi.org/10.3189/2015AoG69A909
Simmonds I, Budd WF (1991) Sensitivity of the southern hemisphere circulation to leads in the Antarctic pack ice. Q J R Meteorol Soc 177:1003–1024
Simmonds I, Jacka TH (1995) Relationships between the interannual variability of Antarctic sea ice and the Southern Oscillation. J Clim 8:637–664

Simmonds I, Li M (2021). Trends and variability in polar sea ice, global atmospheric circulations, and baroclinicity. Annals of The New York Academy of Sciences. Special Issue: The Year in Climate Science Research, 1–20. https://doi.org/10.1111/nyas.14673.

Simmons AJ, Poli P, Dee DP, Berrisford P, Hersbach H, Kobayashi S, Peubey C (2014) Estimating low-frequency variability and trends in atmospheric temperature using ERA Interim. Q J R Meteorol Soc 140:329–353. https://doi.org/10.1002/qj.2317

Stroeve JC, Kattsov V, Barrett A, Serreze M, Pavlova T, Holland M, Meier WN (2012) Trends in Arctic sea ice extent from CMIP5, CMIP3 and observations. Geophys Res Lett 39:L16502. https://doi.org/10.1029/2012GL052676

Sun J, Wang H, Yuan W (2009) A possible mechanism for the co-variability of the boreal spring Antarctic Oscillation and the Yangtze River valley summer rainfall. Int J Climatol 29:1276–1284

Thomson AM, Calvin KV, Smith SJ, Kyle GP et al (2011) RCP4.5: a pathway for stabilization of radiative forcing by 2100. Clim Change 109:77–94. https://doi.org/10.1007/s10584-011-0151-4

Turner J, Bracegirdle TJ, Phillips T, Marshall GJ, Hosking JS (2013) An initial assessment of Antarctic sea ice extent in the CMIP5 models. J Clim 26(5):1473–1484. https://doi.org/10.1175/JCLI-D-12-00068.1

Turner J, Hosking JS, Bracegirdle TJ, Marshall GJ, Phillips T (2015) Recent changes in Antarctic Sea Ice. Phil Trans R Soc A 373(20140163):1–13

Uotila P, Holland PR, Vihma T, Marsland SJ, Kimura N (2014) Is realistic Antarctic sea-ice extent in climate models the result of excessive ice drift? Ocean Modell 79:33–42. https://doi.org/10.1016/j.ocemod.2014.04.004

Weeks WF (2010) On Sea Ice, Fairbanks. University of Alaska Press, Alaska

Wu B, Zhang R, Wang B (2009a) On the Association between Spring Arctic Sea Ice concentration and Chinese Summer rainfall: a further study. Adv Atmos Sci 26(4):666–678

Wu B, Zhang R, Wang B, D'Arrigo R (2009b) On the association between spring Arctic sea ice concentration and Chinese summer rainfall. Geophys Res Lett 36(L09501):1–6. https://doi.org/10.1029/2009GL037299

Xue F, Guo P, Yu Z (2003) Influence of Interannual variability of Antarctic sea ice on summer rainfall in Eastern China. Adv Atmos Sci 20(1):97–102. https://doi.org/10.1007/BF03342053

Xulu N, Chikooree H, Bopape MM, Nethengwe NS (2020) Climatology of the Mascarene High and Its Influence on Weather and Climate over Southern Africa. Climate 8(86):1–11. https://doi.org/10.3390/cli8070086

Yang CY, Liu J, Hu Y, Horton RM, Chen L, Cheng X (2016) Assessment of Arctic and Antarctic sea ice predictability in CMIP5 decadal hindcasts. Cryosphere 10:2429–2452. https://doi.org/10.5194/tc-10-2429-2016

Yuan X, Martinson DG (2000) Antarctic sea ice extent variability and its global connectivity. J Clim 13:1697–1717

Zhang S, Zeng G, Yang X, Iyakaremye V, Hao Z (2021) Connection between interannual variation of spring precipitation in Northeast China and preceding winter sea ice over the Barents Sea. Int J Climatol. https://doi.org/10.1002/joc.7343

Zhao X, Buwen D, Lu R (2021) Interdecadal weakening of the cross-equatorial flows over the Maritime Continent during the boreal summer in the mid-1990s: drivers and physical processes. Clim Dyn 57:55–72. https://doi.org/10.1007/s00382-021-05692-1

Zhou B, Xu M, Sun B, Han T, Cheng Z (2021) Possible role of Southern Hemispheric sea ice in the variability of West China autumn rain. Atmos Res 249(1053329):1–8

Zunz V, Goosse H, Massonnet F (2013) How does internal variability influence the ability of CMIP5 models to reproduce the recent trend in Southern Ocean sea ice extent? Cryosphere 7(2):451–468. https://doi.org/10.5194/tc-7-451-2013